Physical-based hydrological modelling to predict soil moisture in a mesoscale catchment in cold climates

By

Keshav Parameshwaran Shankara Mahadevan

A thesis submitted to the Faculty of Graduate Studies in partial fulfilment of the requirements for the degree of Master of Science

Department of Civil Engineering

Faculty of Engineering

University of Manitoba

Winnipeg, Manitoba, Canada

May 2022

ABSTRACT:

Knowledge of soil moisture is significant for supporting agricultural production and other ecosystem services in cold climates. Climate change is expected to produce more fluctuations in precipitation across the globe and cause more frequent extremes in soil moisture, including floods and drought which have major impacts on agriculture and infrastructure. Forecasting can help mitigate the impacts of soil moisture extremes by providing warnings about upcoming extreme events and prompt mitigation measures. This study constructed a physically-based groundwater-surface water model for an agriculturally dominated watershed in the Red River Valley, Manitoba, to determine the soil moisture variability in a cold climate in deeper soil layers. A 1D replica of the main watershed model was additionally used for sensitivity analysis of soil hydraulic parameters that influenced moisture at different depths. Historically available soil moisture data and additional data from installed Sentek probes in observational fields were used for calibration. Statistical analysis was performed by comparing simulated and measured soil moisture. At the surface (5 cm), the sand series in the 1D model had an excellent match and the 3D results produced a good correlation at the surface during calibration and forecasting. The model results of the deeper layers in the clay soils also showed a good fit during calibration and forecasting while the sand series showed poor correlation at lower depths. The modelling framework in this study provides valuable insights into different hydrological processes.

Acknowledgements

I want to wholeheartedly thank my supervisor Dr Hartmut M. Holländer who was extremely supportive, patient and whose door was always open whenever I faced a roadblock during my research.

I would like to express my deepest gratitude to my co-supervisor Dr Paul R. Bullock who was always patient in teaching me necessary concepts during the research work.

I would like to sincerely thank my advisory committee member Dr Steven K. Frey who was instrumental in making this model and without his passionate teaching and constant input, the model could not have been successfully developed.

I would like to thank my advisory committee member Dr Timi Ojo for his input during the research.

I wholeheartedly thank the Canadian Agricultural Partnership (CAP) and Aquanty Inc., for providing funding for my research work. Thank you to laboratory technician, Kerry Lynch who helped with field planning. Thank you to Madison Stafford for assistance with the field work.

Lastly, I express my very profound gratitude to my parents for providing me with unfailing support and encouragement throughout my years of study. This accomplishment would not have been possible without them. Thank you.

Contributions of Authors

Keshav Parameshwaran S., Dr Hartmut M. Holländer, Dr Paul R. Bullock, Dr Steven K. Frey and Dr Timi Ojo

Physical-based hydrological modelling to predict soil moisture in a mesoscale catchment in cold climates

a) Keshav Parameshwaran S: Developed the fully integrated model, gathered all data and completed data analysis and is the main writer of the paper.

b) Hartmut Holländer: Supervised the research, assisted in data analysis, and with writing and editing of the paper.

c) Paul Bullock: Co-supervised and assisted with the writing and editing of the paper.

d) Steven Frey: Assisted with developing the model and also with writing and editing the paper.

e) Timi Ojo: Assisted with data collection, writing and editing of the paper.

Table of Contents

List of Tables

List of Appendix A Tables

List of Figures

List of Appendix B Figures

Chapter 1 - Introduction

1.1 Motivation

The annual Manitoba Agriculture reports from 2010 to 2021 consistently implied the challenging conditions for the crops to grow because of either excess or lack of water (Crop report 2010; Crop Report Summary 2021; Manitoba Agricultural Services Corporation (MASC) 2021). It is because the climate and its related processes are extremely variable. Scientists and engineers with several technological advancements are coming up with solutions every day to make the conditions for crops growth easier. Soil moisture (SM) is one such process that is highly variable both spatially and temporally and it impacts a range of environmental processes in a nonlinear manner (Western et al. 2002). It plays a major role in climate-change projections by providing feedback at local, regional, and global scales (Seneviratne et al. 2010). Hydrological modelling engineers are interested in water movement and solute transport (Romano 2014) while soil scientists concentrate on SM as water holding capacity and volume of water within the rooting zone (Martínez García et al. 2014; Romano 2014). This study answers scientific questions for both stakeholders. The relationship between mean soil water content and its variance has gathered attention because a clear pattern could be observed (Cornelissen et al., 2013) and those patterns provide a background to discover how different processes contribute to spatial variability of SM.

1.2 Importance of soil moisture in agriculture

Manitoba was once covered in perennial grasses, which created a buildup of carbon in the soil. High carbon content in soil assists in better water infiltration and strong water retention capacity. The Red River Valley in Manitoba is dominated by agricultural fields (Ojo et al. 2015) and the land use for agriculture over the years might have impacted and altered the topsoil and, in turn, influenced the spatial and temporal distribution of SM. SM has a serious influence on agriculture

crop production and yield outcomes and it is also a vital factor affecting greenhouse gas emissions from agricultural soil (Mazrooei et al. 2020). SM is considered to be a dominating factor affecting greenhouse gases like N_2O emissions from the soil as saturated soil tends to increase N_2O production and emissions from cropland soils (Gao et al. 2014). Kuang et al. (2019) highlights the importance of SM and fertilizer application in controlling the benefits of stabilized urea to reduce N_2O production and emissions from the soil. Forecasting accurate SM can support the planning and management of water resources and can significantly assist decision-making for agricultural management. Reliable prediction of deeper layer SM is meaningful for reducing drought damages and economic losses in agricultural production (Zhu et al. 2021). It also assists farmers with optimizing irrigation application to increase crop yield and minimizing redundant irrigation costs.

1.3 Objectives

The objective of this study is to provide a comprehensive analysis of spatiotemporal variability of SM in a mesoscale catchment located in a hydrologically complex setting within the Red River Valley in Manitoba, Canada, by developing a fully functioning physically based surface water - groundwater model. Another integral focus of this study is to predict SM over deeper depths and analyze the prediction correlation with measured SM data for the 2021 growing season.

Chapter 2 - Literature Review

2.1 Different approaches for measuring soil moisture

Dorigo et al. (2015) evaluated a new, merged SM product that combines the SM retrievals from four passive and two coarse resolution microwave sensors into a global data set spanning the period 1979 to 2010. The evaluation uses ground-based SM observations of numerous study sites. The triple collocation technique was used in the study to assess random errors in the data set. The difference in the Spearman correlation coefficient between the new SM product and all in-situ observations was small but differences between networks and time periods were large. The RMSE differences and triple collocation errors showed lesser variation between networks. Apart from differences in spatial scale, neither the sensing depth of the SM product nor the installation depth of sensors was uniform. This led to uncertainties in the evaluation results. The literature highlighted that there was a strong relationship between remotely sensed surface soil moisture and in-situ measurements in the upper soil layer. The highlight could be a limitation for a study that involves measuring SM at deeper depths.

Ojo et al. (2015) investigated the design of an SM network and the calibration of Stevens Hydra Probe sensors (Stevens Water Monitoring Systems 2008) in the Red River Basin, Manitoba, and evaluated their performance. The established SM network provided real-time information on SM conditions within the root zone in an agricultural area prone to SM extremes. The SM network called RISMA (Real-Time In-situ Monitoring for Agriculture) evaluation sites consisted of nine locations with coarse and fine-textured soils where the sensors were installed horizontally in triplicate at 5, 20, 50 and 100 cm and soil samples from the same location were preserved for laboratory calibration. Data from three other fields (outside the RISMA network) were collected to provide the reliability of the overall field calibration equation developed from the sites within

the network. The results of laboratory calibration underestimated the SM at the three sites outside the network. However, both the in-situ and overall field calibrations performed better than the default sensor calibration at the RISMA sites. The greatest advantage is it provides the most accurate SM input values possible which can be assessed with remotely sensed products. A drawback of using the sensor for volumetric water content determination is its sensitivity to temperature and salinity resulting from its low operating frequency.

Cho et al. (2015) highlighted the importance of large-scale observation of root zone SM data using remote sensing. The study validated the Advanced Scatterometer (ASCAT) and the Advanced Microwave Scanning Radiometer - Earth Observing System (AMSR-E) sensor products. The results of the surface SM products showed a reasonable agreement with average correlation coefficient values. The root zone SM derived using the soil water index showed relatively high values at a depth of 20 cm. The best results were observed at 20 cm depth and based on the results, ASCAT SM products were shown to be potentially more appropriate than AMSR-E products in the study area.

2.2 Current research in soil moisture forecasting

Zhu et al. (2021) is one of the very few publications which discusses multi-layer SM prediction over an agriculturally dominated catchment, however, it uses data-driven methods like support vector machines (SVM) and data-assimilation algorithms like the ensemble Kalman filter (EnKF) rather than hydrological modelling. The study investigated the performance of SVM and coupled SVM-EnKF in predicting SM in multi-layers (0-5, 0-10, 10-40 and 40-100 cm) by adding three remote sensing SM products namely Soil Moisture Active Passive (SMAP) (Bhuiyan et al. 2018), passive AMSR and active ASCAT (Cho et al. 2015) separately. The input meteorological variables were collected from 14 weather stations. The results of SVM on its own produced satisfactory

results for surface layer SM prediction and poor results for root layers. The addition of SMAP with SVM improved the prediction results while the addition of the other two SM products did not show any improvement. SVM-EnKF coupling produced the best results and adding any of the remote sensing techniques to SVM-EnKF did not improve the results any further. It was stated in the study that techniques like SVM are better in SM prediction for multi-layers when compared to physically-based techniques, however, it did not provide a comparison of results. A slight advantage of using such techniques is that it requires relatively fewer input variables for SM prediction than physical-based models.

Mazrooei et al. (2020) developed monthly to seasonal (M2S) top layer SM forecasts. The SM forecasting skill was evaluated in comparison with the remotely sensed SM observations collected by the SMAP satellite (Bhuiyan et al. 2018). The rain-fed crops depend on SM conditions during the growing phase, hence a SM forecast would help determine the crop yields. This study exploited the SMAP data to validate the M2S SM forecast. The Noah3.2 Land-based Model (LSM) ran the SM simulations and gave SM forecasts over the study area. Meteorological variables like precipitation, wind speed, net short-wave radiation which are needed to forecast SM were implemented in the LSM. Mean monthly SM forecasts of the top 10 cm layer of the soil were computed by averaging daily forecasted SM quantities. Monthly SM forecasts were compared with corresponding monthly time series of SMAP observations using correlation coefficient and RMSE which helped to quantify the forecasting skill. The study indicated that most SM forecasting scenarios were predominantly influenced by updating the initial conditions before forecasting. One drawback was the decline in the skill of the SM forecast with increasing lead time due to errors in the prediction of other meteorological variables like precipitation. The results in the study showed decent accuracy. Uncertainty in SMAP data was another major drawback so a comprehensive

assessment of forecasting skills could not be achieved. The future scope of this study can be done by using different hydrological models to forecast SM for a shorter period where the weather forecast can be predicted more accurately.

2.3 Influence of soil hydraulic parameters on soil moisture

Maheu et al. (2018) wanted to emphasize the limitations of the Soil, Vegetation and Snow (SVS) land surface model by comparing its performance with HydroGeoSphere (HGS) (Therrien et al. 2010). Both the models were set up to perform 1D soil column simulations. To identify the variations, key differences between soil hydraulic properties were used by both models. Hydraulic conductivity (K) was assumed to exponentially decay with depth in SVS while it was set up as constant in HGS. HGS simulations derived K and residual saturation (θ_r) using soil texture as an input to the Rosetta model (Schaap et al. 2001). Final results indicated that under Mediterranean and temperate climates, SVS satisfactorily simulated SM, with a performance comparable to HGS. However, SVS performed weakly under a semiarid climate while HGS performed relatively well. Also, HGS was able to simulate SM decline during the summer and spring months when the vegetation was active. The HGS model fared much better than SVS at deeper soil layers as they were able to capture θ_r during the dry periods. HGS simulations captured the observed variability in SM at the middle soil layer, but reduced performance was observed at the bottom soil layer.

An et al. (2018) established a surrogate-based simulation optimization approach to identify parameters values for a fully integrated surface water and groundwater flow coupling simulation. They used the HGS model and a local sensitivity analysis method and emphasized a few parameters of extreme importance. The importance was determined by the influence of parameters on the simulation model. The results showed that hydraulic conductivity, the porosity of the soil, van Genuchten parameters, and the Manning coefficient exerted a large influence on the model

output. Hence, the four parameters were provided high priority during the HGS model parameter identification process in the study.

Martínez García et al. (2014) focused on SM with and without root water uptake using water flow simulations. It was performed by varying the soil hydraulic properties under different climatic conditions. The study explained the differences in positive or negative relationships observed between mean SM and its variability. The study also assisted in specifically targeting spatial variability of K and measure of pore-size distribution index (n) in the van Genuchten model. The model created was 1D, K was the only parameter that was constantly varied and the rest of the drivers like rainfall, evaporation, Evapotranspiration (ET) were kept homogenous. However, the study failed to evaluate how SM varies with heterogenous weather patterns, as it might impact the vegetation development and in turn influence the soil hydraulic properties.

2.4 The capability of HGS

Brunner and Simmons (2012) described in detail the exact working of the HGS model and the functions it can perform. HGS can solve both simple (steady-state saturated flow) as well as complex (integrated flow solute) problems. It is applied to a wide range of hydrological problems like watershed modelling, disconnection between surface and groundwater, fractured rock hydrology, simulation of the fate of contaminants in groundwater and atmospheric/surface/sub-surface heat exchange processes. HGS can simulate water flow in a fully integrated mode, hence allowing precipitation partitioning into all key components of the hydrologic cycle which is the most important aspect of HGS. It is structured as a control volume finite element model for both surface and sub-surface domains. One drawback is that it does not have a Graphical User Interface (GUI). Learning TECPLOT along with HGS creates a steeper learning curve. Also, multiple functions are not documented which limits user utilization of the full numerical capability of the

model. However, the user can change a range of numerical parameters during the simulation. The learning curve is fairly simple for problems that are not too complex. However, for this research, the learning curve is much steeper since it involves a complex regional-scale catchment under hydrologically challenging conditions.

2.5 Using HGS to determine soil moisture

Cornelissen et al. (2013, 2014, 2016) were the main references for this research since they provided information on simulating SM using the HGS. Cornelissen et al. (2013) applied HGS in a natural ecosystem to assess whether the model can simulate the pattern of SM. The study aimed to analyze whether the 3D simulation (θ_{sim}) reproduces statistical measures of the observed SM (θ_{obs}) pattern. HGS provided SM patterns at different spatial resolutions. Climate data including precipitation data were considered as input parameters that were collected from meteorological stations. The initial aim of the model calibration was to get a good fit between $\theta_{sim\ and}\ \theta_{obs.}$ The aim was achieved by altering the canopy storage parameters, transpiration and soil porosity values. The results of the simulation of two chosen resolutions showed that the low flow period was well captured by both resolutions but peaks during the same time were not captured. HGS overestimated discharge during the calibration period but produced better simulation results during the validation period. The simulation did not capture the short-term dynamics of SM at 50 cm. It reproduced some parts of the short-term dynamics at 20 cm depth and overestimated the dynamics at 5 cm depth. The dynamics at 20 and 50 cm depth resulted from the vertical flow components due to bypass flow occurring in spruce covered catchments that were not simulated by the model. The study stated that the simulation of SM was successful only for the 20 cm depth. A decrease in SM variance during continued drying was observed for both simulations and the measurements for both resolutions. In addition, the pattern of θ_{obs} showed a patchy character that did not show in the θ_{sim}

indicating that using uniform soil properties in the topsoil makes the SM simulation inaccurate. The θ_{obs} pattern looked patchy while the θ_{sim} was dependent on topography.

Cornelissen et al. (2016) improved their previous study, where they dealt with one major limitation to the application of HGS at mesoscale catchments. The available database was insufficient for calibration as HGS required a large amount of data for simulations. This is one of the newest studies done which answered how to tackle a limitation in HGS. The study parameterized the distributed model for a mesoscale catchment by transferring model-specific parameters calibrated for water balance and SM dynamics at a small headwater catchment. The effect of the parameterization was differentiated from the influence of spatial variability in land use, soil, PET and precipitation by introducing their spatial distributions in a model setup. For the spatial variability in land use at the catchment, parameters that are not model specific (e.g. LAI, root depth and root distribution) were taken from the scientific literature.

Chapter 3 – Physical-based hydrological modelling to model and predict soil moisture in a mesoscale catchment in cold climates

Preface

This chapter contains a detailed description of constructing a physical-based hydrological model to simulate soil moisture for an agriculturally dominated catchment. It modelled and predicted soil moisture from surface to deep root zone layers for different textural classes of soil under hydrologically challenging conditions. This study provides insights into the extent of soil hydraulic parameters, lateral movement of water and how it influences the soil moisture variability in different soil types. The model achieved good correlations between modelled results and the historically available results of the catchment in consideration.

3.1. Introduction

Soil Moisture (SM) is a vital variable in the soil-plant-atmosphere system (Cornelissen et al. 2014; Rong et al. 2017). It fluctuates in space and time (Rosenbaum et al. 2012) and is governed by interacting environmental factors like soil properties (Vereecken et al. 2008), vegetation (Schwärzel et al. 2009), topography (Cantón et al. 2004), precipitation (Cornelissen et al. 2013). The SM pattern tends to change because of non-uniform precipitation, incoming solar radiation, and other soil and vegetative properties (Srivastava et al. 2020). Dynamic patterns of variation of SM in farmed catchments have gathered attention in recent times (Cornelissen et al. 2013). For agricultural crops, SM content directly affects their successful production through its impact on the trafficability of fields for fieldwork (Müller et al. 2011), crop water availability and yield (Raddatz et al. 1994), the level of pest pressure (Mila and Yang 2008) and the potential for soil compaction with the use of agricultural implements (Alakukku et al. 2003). Farmed catchments

display higher spatio-temporal heterogeneity of SM because of agricultural practices (Hébrard et al. 2006; Motisi et al. 2012; Rallo et al. 2012). However, only a few studies have focused on SM variability in farmed catchments (e.g. Hawley et al. 1983; Hébrard et al. 2006) and our understanding of SM variability at the catchment scale is limited because of on-field measurement constraints (Meng et al. 2021; Rosenbaum et al. 2012; Srivastava et al. 2020).

SM data is a critical step in model initialization for weather forecasting in cold climates, agricultural planning, and water resources management and it has a major impact on agricultural crop production and yield outcomes (Liu et al. 2020). Present and future SM data are invaluable for many practical and academic uses (Meagher 2017). Forecasting SM helps to predict and monitor natural disasters such as floods (Srivastava et al. 2016; Wasko et al. 2020), drought (Van Hateren et al. 2021; Zhang et al. 2017), wildfires (Chaparro et al. 2016), landslides (Krzeminska et al. 2012) and severe weather events (Raddatz and Cummine 2003). It will also assist in enhancing early warning systems related to famine, and supports evaluation of ground suitability for civil engineering purposes all over the world (Chifflard et al. 2018; Meagher 2017). It is extensively recognized in the scientific community that an enhanced understanding of SM dynamics can yield valuable insights into hydrogeological processes in cold climates (Blume et al. 2009; Rosenbaum et al. 2012; Vereecken et al. 2008; Zehe et al. 2010).

The SM measuring techniques such as in situ measurements, installation of numerous spatially distributed SM sensors, interpolation using statistical models is time-consuming, laborious, and/or expensive (Chifflard et al. 2018; Vereecken et al. 2008). Hence major efforts to optimize SM networks are required (Li et al. 2011; Richardson et al. 2008; Sunohara et al. 2015). Hydrological modelling can provide accurate, cost-effective, and efficient frameworks for encapsulating spatio-temporal processes (Frey et al. 2021). Previous studies have emphasized the need for process-

based modelling in addition to various methods already available to test theories on hydrological processes influencing SM distribution (e.g. Chen et al. 2018; Lee et al. 2018; López-Ballesteros et al. 2019; Moriasi et al. 2006; Oliveira et al. 2020). The dynamic and spatially explicit hydrological models help to relax many of the restrictive assumptions made in statistical models. Physically-based, fully-integrated, groundwater-surface water models where the surface water system is dynamically coupled to the groundwater flow system, are arguably the most advanced tools for simulating large-scale hydrological processes (Berg and Sudicky 2019; Fatichi et al. 2016; Frey et al. 2021). Despite the availability of spatially distributed remote sensing derived SM data, clear analysis and comparison of simulated SM with catchment-scale physically-based hydrological models are rare (Herbst and Diekkrüger 2003; Mahmood and Vivoni 2011; Rößler and Löffler 2010; Tavakoli and De Smedt 2012; Zhang and Wegehenkel 2006). Due to high computational demand, integrated hydrological models like HydroGeoSphere (HGS), are used predominantly for small-scale applications. Attempts to use HGS for studies having large agriculturally dominated catchments are only found occasionally (e.g. Goderniaux et al. 2009; Rahman et al. 2014). Cornelissen et al. (2016) and Rong et al. (2017) stated that previous research contained limited insight into the spatial and vertical distribution of SM in a catchment. Vereeken et al. (2008) stated that deeper soil profile measurements are typically not concentrated in general SM studies. However, hydrologic science requires insight on SM conditions in deeper soil layers in cold climates as it provides information on hydrological fluxes. Mazrooei et al. (2020) highlighted that detailed research is necessary for forecasting SM as there are various knowledge gaps and lower accuracy in predicting SM at different depths.

The objective of this study is to provide a comprehensive analysis of spatiotemporal variability of SM in a mesoscale catchment located in a hydrologically complex setting within the Red River

Valley in Manitoba, Canada, by developing a fully functioning physically based surface water - groundwater model. Another integral focus of this study is to predict SM over deeper depths and analyze the prediction correlation with measured SM data for the 2021 growing season. The results of this research will provide valuable support to various systems which can utilize present and future SM data as prime input.

3.2 Materials and Methods

3.2.1 Study Area

The Brunkild sub-catchment is in south-central Manitoba, Canada. The study area is approximately 72 km southwest of the city of Winnipeg (Fig. 1). The Brunkild sub-catchment in the Red River Valley has an area of 508.96 km^2. The landscape is generally flat to gently undulating with slopes from 0 - 2% through most of the sub-catchment and steeper slopes on the Manitoba escarpment to the west. It provides a mix of land covers, although land use is dominated by annual cropping (Bhuiyan et al. 2018). Crops grown in this region include forage, sunflower, corn, spring wheat, soybean, and canola. Field size varies from 40 to 260 hectares in area with 65 ha being common. This region is characterized by a wide range in soil texture (Walker 2012) with coarse, sandy soils extending from the Manitoba escarpment on the west to a sharply-defined boundary with fine, heavy clay soils in the Red River Valley on the east.

Four observation fields located inside the study area (Fig. 2) were selected based on the triplet aspect (Romano 2014; Vereecken et al. 2008; Western et al. 2002) of local scale, namely support, spacing and extent. The first two fields were those where the Real-time In-Situ Soil moisture Monitoring for Agriculture (RISMA) stations 4 and 5 are located at the sand-clay interface in the catchment and are referred to as RISMA 4 and RISMA 5 (Table 1). The RISMA 4 and 5 stations

monitor air temperature, relative humidity, wind speed and direction, rainfall as well as SM. Three replicate Hydraprobe II frequency domain reflectometer sensors (Stevens, Oregon, USA) were installed at 5, 20, 50 and 100 cm depths. Two Sentek SM probes (Stepney, South Australia) were installed in two different agricultural fields after the crops were planted in 2020 and 2021 then removed prior to harvest each year (Fig. 2); one was sandy-textured (Sentek sand) and one was heavy clay (Sentek clay) (Table 1). They are fully encapsulated "drill and drop" probes, 90 cm in length with SM sensors for each 10 cm increment that were completely buried in the soil. The Sentek sensors were connected to a data logger which recorded SM on an hourly basis and transmitted real-time data to an online cloud platform.

Table 2 shows the soils series for these four fields (Michalyna et al. 1988) and the crops grown in 2020 and 2021. Scanterbury (SCY) soils are developed from lacustrine deposits and have clay to heavy clay texture, high available water holding capacity and slow permeability. Kronstal (KOT) soils formed from lacustrine deposits and have coarse loamy texture, medium available water holding capacity, moderately rapid permeability and a water table between 1 to 2 m from the surface during the growing season. Willowcrest (WWC) soils developed from lacustrine deposits and have sandy texture, low available water holding capacity, moderately rapid permeability and a water table between 1 to 2 m from the surface during the growing season.

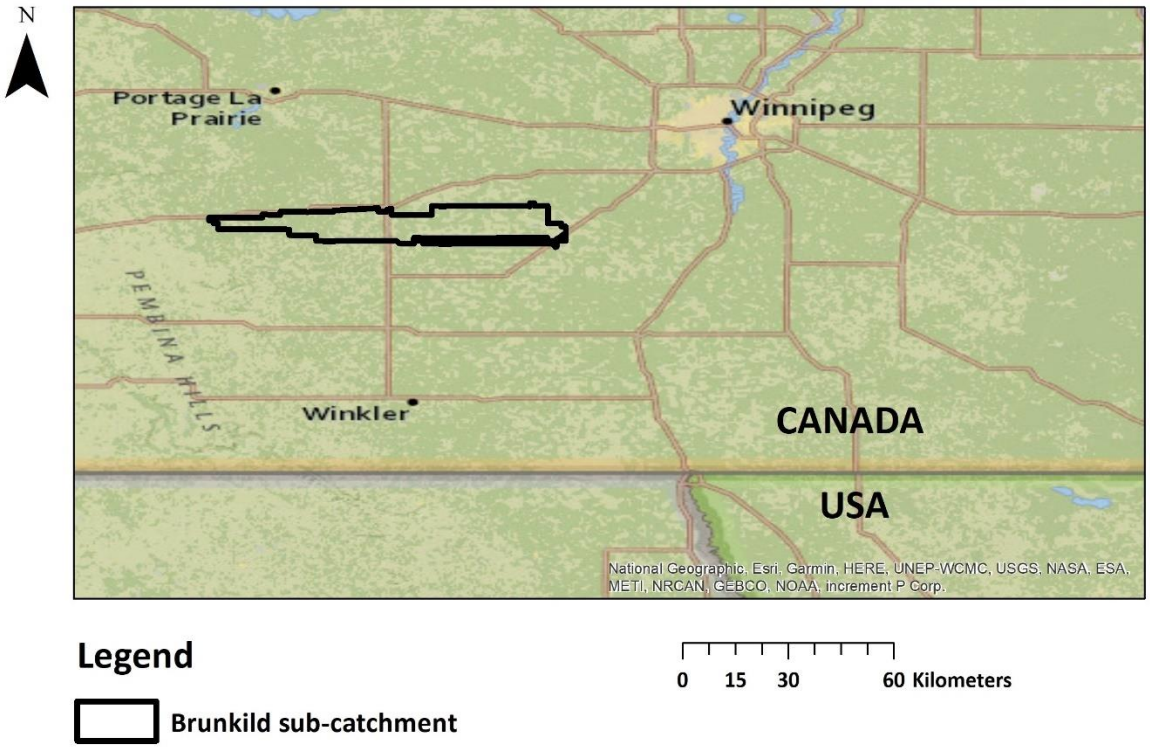

Fig. 1: Brunkild sub-catchment in south-central Manitoba, with respect to the city of Winnipeg, Canada.

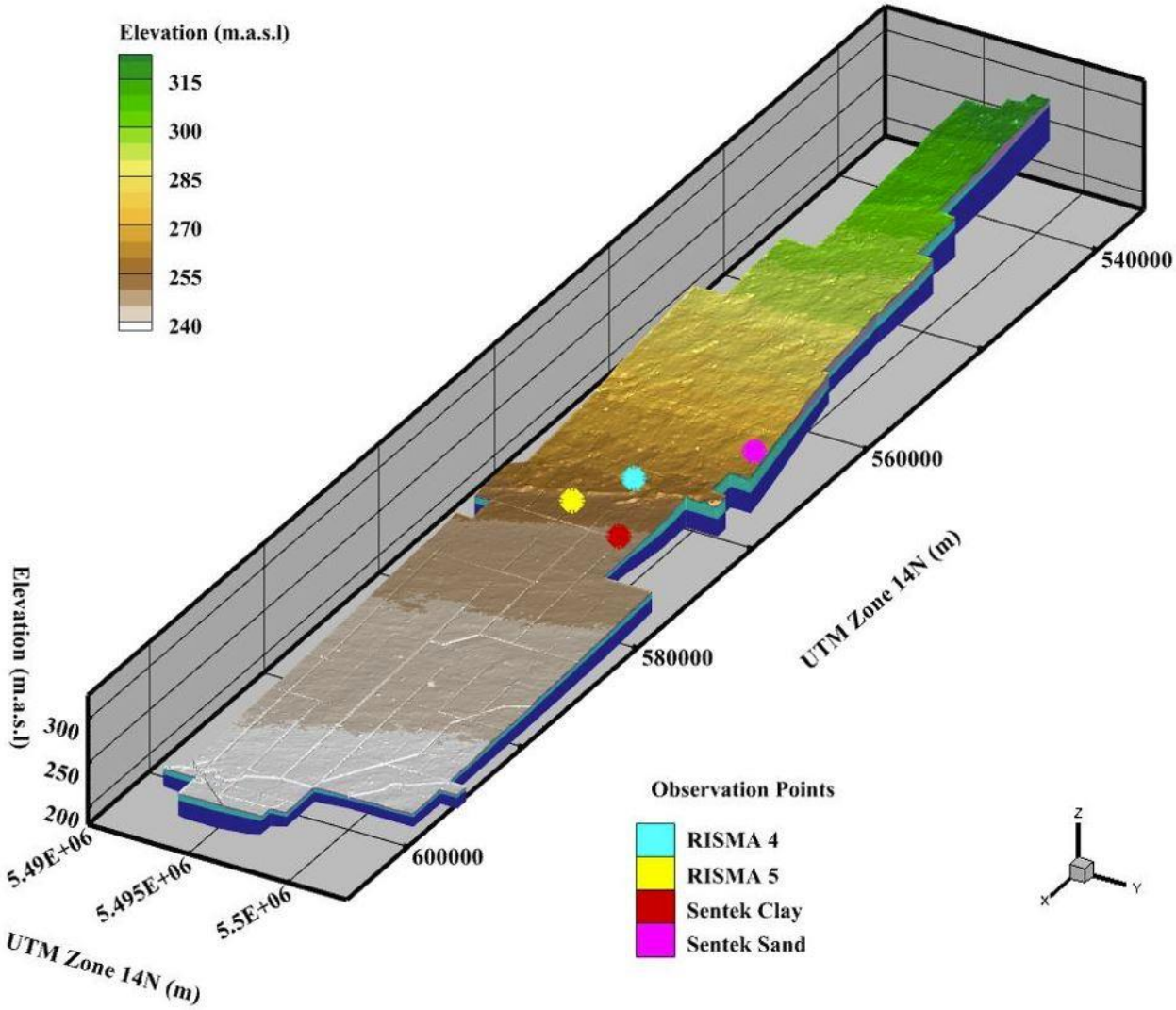

Fig. 2: HGS three-dimensional (3D) model of Brunkild sub-catchment and observation fields in the study.

Table 1. Observation field locations and elevations.

Station name	X coordinate	Y coordinate	Elevation (m a.s.l)[1]
Sentek sand	568406.63	5502311.00	265.00
Sentek clay	576766.36	5500257.51	249.00
RISMA 4	573012.46	5498788.11	259.00
RISMA 5	575275.50	5497070.50	252.00

[1] Above sea level

Table 2. Observation fields with the soil series at the monitoring station and the crops grown during the study.

Station name	Soil Series[1]	Crop 2020	Crop 2021
Sentek sand[2]	Willowcrest	Soybean	Corn
Sentek clay[2]	Scanterbury	Canola	Wheat
RISMA 4[3]	Kronstal	Canola	Corn
RISMA 5[3]	Scanterbury	Soybean	Wheat

[1]Michalyna et al. 1988

[2]Sentek field sensors were installed June through August 2020 and May through August 2021

[3]RISMA stations were installed in 2012 and became operational in 2013

The crops grown at RISMA 4 and 5 preceding 2020 are listed in Table A.1.

3.3 HydroGeoSphere (HGS)

The physically-based fully-integrated model used for the study is HydroGeoSphere (Therrien et al. 2010). HGS can simulate soil moisture variability in three dimensions (Brunner and Simmons 2012). A preprocessor named GROK prepares the input files. Once the simulation is terminated, a postprocessing program converts the output data to a format that can be read by third-party visualization packages such as TECPLOT (Tecplot Inc 2011).

3.3.1 Overland flow

The two-dimensional surface domain is coupled directly over the three-dimensional domain by a dual node approach and is modelled by the diffusion wave simplification of the Saint-Venant equation:

$$\frac{\partial \emptyset_0 \, h_0}{\partial t} = \nabla\big(d_0 K_0 \nabla(d_0 + z_0)\big) + d_0 \Gamma_0 + Q_0 \qquad (1)$$

where $Ø_0$ is the porosity of the surface domain [-], h_0 is the water surface elevation [L], d_0 is the surface water depth [L], t is the time [T], Γ_0 is the surface water volumetric exchange between domains [$L^3\ L^{-3}\ T^{-1}$], Q_0 is the total contribution of surface domain sources [$L\ T^{-1}$], and K_0 is the surface water conductance [$L\ T^{-1}$].

3.3.2 Subsurface flow

HGS utilizes a modified form of Richard's equation to describe three-dimensional transient subsurface flow in a variably-saturated porous medium:

$$-\nabla(\omega_m q) + \Sigma\, \Gamma_{ex} \pm Q = \omega_m \frac{\partial\,(\theta_s S_w)}{\partial t} \tag{2}$$

where ω_m is the volumetric fraction of total porosity occupied by porous medium [-], Γ_{ex} is the volumetric water exchange flux between domains [$L^3\ L^{-3}\ T^{-1}$], Q represents the total contribution of sources [$L^3\ L^{-3}\ T^{-1}$], q is the fluid flux [$L\ T^{-1}$] and is given by

$$q = -K \times k_r \nabla(\psi + z) \tag{3}$$

where K is the hydraulic conductivity [$L\ T^{-1}$], k_r is the relative permeability [-], ψ is the pressure head [L], z is the elevation head [L]

The hydraulic conductivity, K [$L\ T^{-1}$], is given by:

$$K = \frac{\rho g}{\mu} k \tag{4}$$

where g is the acceleration due to gravity [$L\ T^{-2}$], is the viscosity of water [$M\ L^{-1}\ T^{-1}$], k is the permeability of porous medium [L^2], and ρ is the density of water [$M\ L^{-3}$].

The saturated water content θ_s [-] is assumed equal to porosity and S_w is the degree of water saturation [-] and is given by:

$$S_w = \frac{\theta}{\theta_s} \quad (5)$$

where θ is the water content [-].

Based on earlier works of Mualem (1976), van Genuchten (1980) proposed the saturation-pressure relation which is incorporated in the HGS model as:

$$S_w = S_{wr} + (1 - S_{wr})\,[1 + |\alpha\psi|^{\beta}]^{-v} \quad \text{for } \psi < 0 \quad (6)$$

$$S_w = 1 \quad \text{for } \psi \geq 0$$

$$\text{where } v = 1 - \frac{1}{\beta} \quad \text{for } \beta > 1 \quad (7)$$

where S_{wr} is the residual water saturation [-], α is the inverse of air-entry pressure head [L^{-1}], β is the pore-size distribution index [-]

3.3.3 Three-dimensional finite element mesh

AlgoMesh (HydroAlgorithmics 2016) was used to generate an unstructured finite element grid. The unstructured grids allow localized regions of interest within the model domain to carry higher spatial resolution. The grid was designed with 5 - 50 m nodal distance along with the main surface drainage features, and up to 150 m nodal distance in areas distal from roadways, channels, and ditches (Fig. 3). A LiDAR-based Digital Elevation Model (DEM) from the Manitoba Land Initiative (MLI) (Manitoba Land Initiative 2001) was used to define the model topography and the subsurface layers were developed using processed raster files that represent the hydrostratigraphic surfaces. The model domain was discretized with 45,929 nodes and 88,566 triangular elements per 2D mesh sheet (367,432 nodes and 708,258 elements in total across the 8-layer subsurface domain).

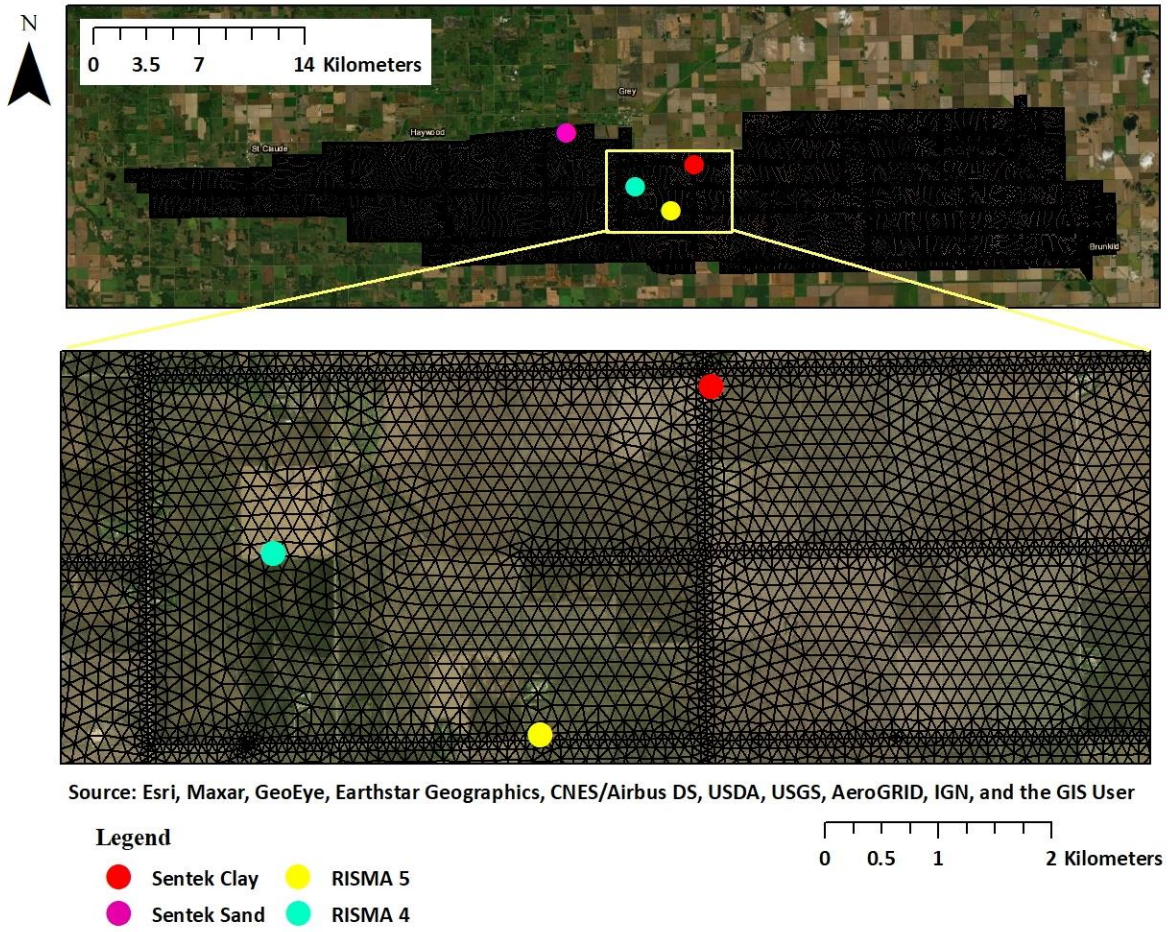

Fig. 3: Plan-view of Brunkild sub-watershed with dense triangular mesh elements (top panel), and the finite element mesh in the area of the three observational fields (bottom panel).

3.3.4 Landcover

The spatially distributed landcover was derived from AAFC 2014 Annual Crop Inventory (Fisette et al. 2013). It includes forests, croplands, wetlands, grasslands, open water, and urban land (Fig. 4). HGS reads the value of pixels from the raster file and assigns transpiration fitting parameters values (C1, C2, and C3), transpiration limiting parameters (wilting point, field capacity, oxic limit, and anoxic limit), Leaf Area Index (LAI), time-varying root density function (RDF) and evaporation limiting factors (evaporation depth, canopy evaporation). The rate of transpiration and the RDF are incorporated into HGS using:

$$T_p = f_1(LAI, C1, C2) f_2(\theta, C3) RDF(t)[E_p - E_{can}] \quad (8)$$

$$RDF(t) = \frac{L_m L_0}{L_0 + (L_m - L_0) e^{-rt}} \quad (9)$$

where T_p is the rate of transpiration [L T^{-1}], f_1 (LAI) and f_2 (θ) are a function of leaf area index and nodal water content respectively, C1, C2, and C3 are dimensionless fitting parameters, L_m and L_0 are maximum root depth and initial root depth respectively, E_p is the reference evapotranspiration [L T^{-1}] and E_{can} is the canopy evaporation [L T^{-1}]. The values of the transpiration parameters were referenced from Kristensen and Jensen (1975) and the evaporation depth from the cropland was kept at 0.2 m implying that water available at 20 cm of the soil profile would be able to directly evaporate. The LAI was calculated using Moderate Resolution Imaging Spectroradiometer (MODIS) data (Myneni et al. 2015) for the Brunkild catchment for the 2010 – 2021 period. The time-varying root depth values for the cropland landcover class were referenced from Canadell et al. (1996).

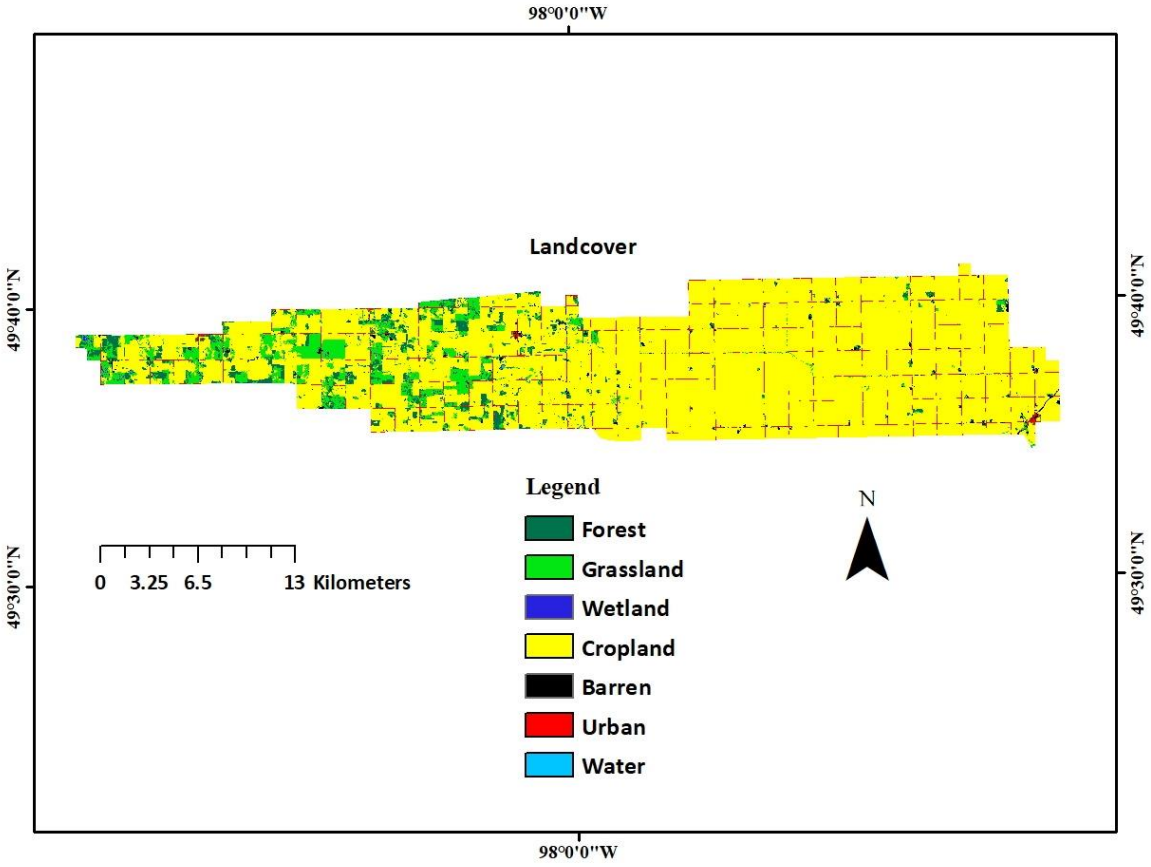

Fig. 4: Spatially distributed land cover resolved in the model.

3.3.5 Hydrostratigraphy

The LiDAR-based DEM obtained from MLI was divided into 4 layers at 5 cm, 20 cm, 50 cm, and 100 cm respectively (Fig. 5). The observed data from the RISMA fields were available only for the aforementioned depths, hence the model topography was divided at the same intervals. There are four more layers below these (Fig. 5b) representing the surficial geology as described in the subsurface phanerozoic geology of southern Manitoba (Transect 15 at UTM 550870N (Matile and Keller 2012)). The subsurface layers were developed using processed raster files. The soil

hydraulic conductivity values of the subsurface layers were derived from existing literature (Freeze and Cherry 1979; Grisak and Cherry 1975; Grisak and Jackson 1978).

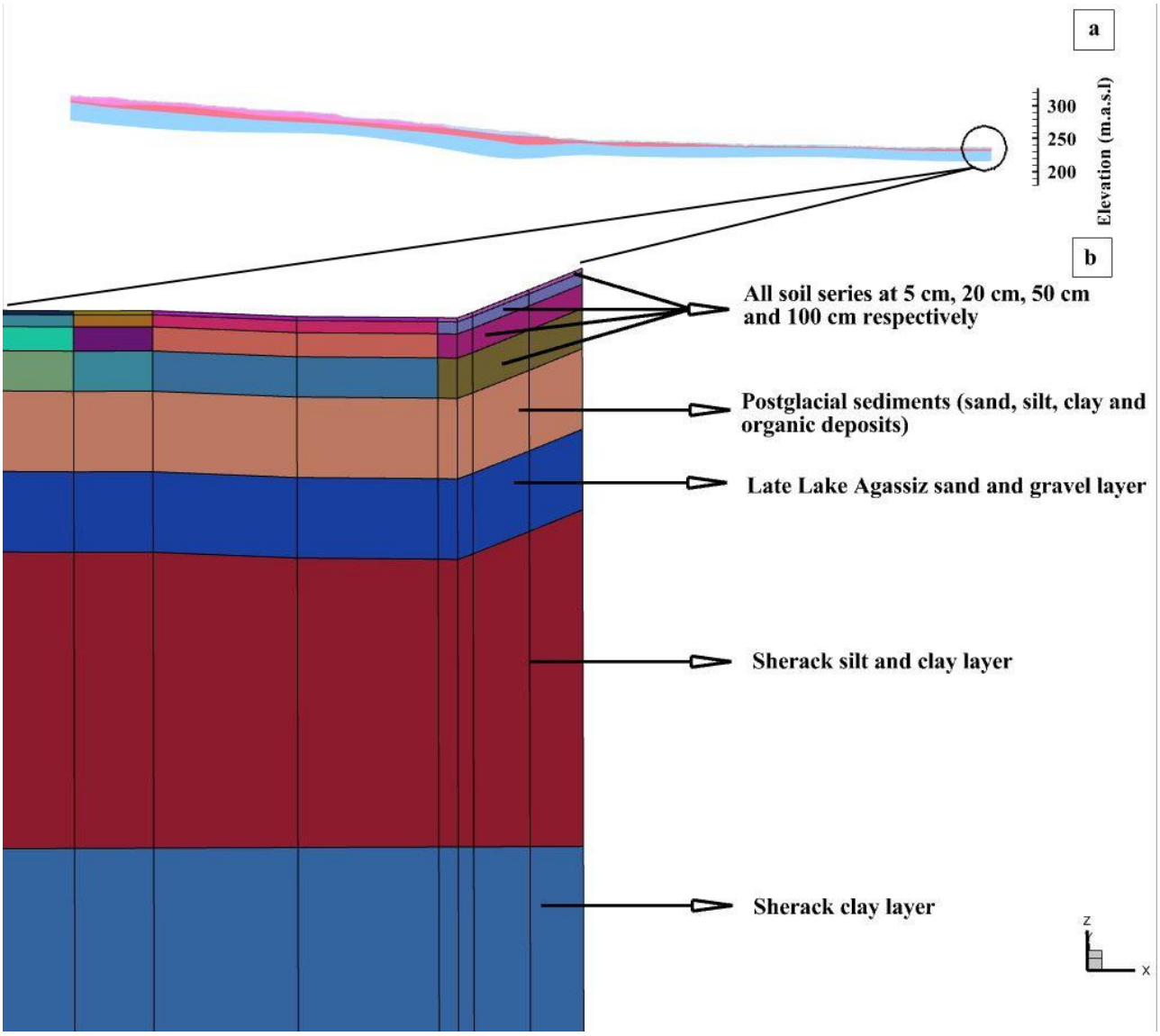

Fig. 5**:** Cross-section of HGS model subsurface phanerozoic geology of Brunkild sub-catchment (a); Description of subsurface layers along with discretization (inset) (b); Details of each subsurface geology layer can be found in Matile and Keller (2012).

3.3.6 Soil

The soil information for the Brunkild sub-catchment was obtained from MLI. MLI provides soil maps of districts in several scales (1: 40,000, 1: 20,000, etc.). The polygons of Brunkild have a constant spatial resolution of 1: 20,000. The total polygon count of the Brunkild sub-catchment is 608 with 33 different soil series (Fig. B.1). Each soil series has individual soil hydraulic parameters. Brunkild is a mesoscale sub-catchment that exhibits substantial spatial variability in soil hydraulic properties. The percentage of sand, silt, and clay along with the bulk density of each soil series (Table A.2) were inputted into Rosetta (Schaap et al. 2001; Zhang and Schaap 2017) and the corresponding parameters results of residual water content (θ_r), saturated water content (θ_s), hydraulic conductivity (K), and van Genuchten-Mualen parameters α (>0) which is related to the inverse of air entry suction and n (>1) is the measure of pore-size distribution index (van Genuchten 1980) were obtained specifically for each soil series. The detailed explanation for individual soil series in Fig. B.1 can be obtained in Michalyna et al. (1988).

3.3.7 Boundary conditions

The liquid water inflow (Neumann) boundary condition was used at top of the model to represent rainfall, snowfall, and Potential Evapotranspiration (PET) (recharge is computed internally by the model). A critical depth boundary condition was applied to the surface nodes around the perimeter of the domain. The perimeter of the subsurface domain and the base of the model were considered as no-flow boundary conditions. Daily frequency liquid water input (precipitation + snowmelt) and PET collected from the RISMA stations were used to establish model conditions and achieve quasi-equilibrium conditions by repetitive simulation runs. The results achieved after year-over-year quasi-equilibrium conditions were used as initial conditions for the subsequent model simulation runs.

3.3.8 Climate forcing data

3.3.8.1 Precipitation and snowmelt

Daily precipitation data (2010 – 2021) were collected from weather stations RISMA 4, 5 (present inside the catchment), RISMA 7 (at the northern border of Brunkild), and Elm creek and Carman stations a few kilometers away from the study area (Table 3). A long period (11 years) of daily climatology data used as forcing data helped the model to forecast accurate SM values. However, there were multiple challenges (unavailability of the source, missing days, etc.) in collecting long-period datasets. The daily snowmelt data were collected from the SNOw Data Assimilation System (SNODAS). The SNODAS data are model output (Niehaus 2015) and the values are stored as raster data files. Each cell represents 1 km^2 spatially and 24 hours temporally. Each grid cell represents the daily average value. The daily snowmelt was extracted from the data files for October to May during the predominant snowmelt period (Table 3).

3.3.8.2 Potential Evapotranspiration (PET)

PET was computed based on the Hargreaves method (Hargreaves and Samani 1985; Sentelhas et al. 2010). It uses only the maximum and minimum temperatures and is expressed by:

$$PET = C_0 \, Ra' \, (T_{max} - T_{min})^{0.5} \, (T + 17.8) \quad (10)$$

where, Ra' is extraterrestrial solar radiation, in [L T^{-1}], C_0 is the conversion parameter (= 0.0023) for near prairie regions in Canada, T is the daily mean air temperature [°C] at 2 m, based on the average of the maximum and minimum temperatures, and T_{max}, T_{min} are the daily minimum and maximum temperatures, respectively [°C].

The Hargreaves method used a minimal number of input climatology variables to calculate PET for the 2010 – 2021 period (Table 3). NASA through its earth science program has developed a beneficial tool named POWER (Prediction Of Worldwide Energy Resources). The POWER platform provides worldwide single point data of both solar and meteorological parameters (Sparks 2018). Hence, the daily Ra, T_{max}, T_{min} over the Brunkild catchment were collected for the 2010 – 2021 time period using NASA's POWER tool.

Table 3: Observational data used to configure model meteorological inputs.

Data	Data availability period	Temporal data consideration	Source of data sets
Precipitation (mm/d)	2010 – 2021	Daily	RISMA stations 4, 5 and 7, Elm Creek, and Carmen
PET (mm/d)	2010 – 2021	Daily	RISMA stations 4, 5 and 7, Elm Creek, and Carmen
Snowmelt (mm/d)	2011 – 2021	Daily	SNODAS[1]
Liquid water influx (mm/d)	2010 – 2021	Daily	-
LAI (-)	2010 – 2021	8-day average	MODIS

[1] The 2010 SNODAS data was unavailable for the Brunkild catchment. The National Operational Hydrologic Remote Sensing Center (NOHRSC) extended the spatial coordinates covering Brunkild only from 2011.

3.3.9 One-dimensional HydroGeoSphere Model

Vereecken et al. (2008) has stated that appropriate model dimensions must be selected that depict the field situation as accurately as possible. For the sake of computation simplicity, SM data are often analyzed using a one-dimensional model (1D) which assumes the flow occurs only vertically

(Vereecken et al. 2008; Vrugt 2001). However, to assess the validity of this assumption a comparison with a multidimensional model is required, which was also done in this study. A relatively simple 1D model with dimensions of 1 m x 1 m x 10 m was created (Fig. 6). The upper soil layers were considered to be similar to the soil series of the observational fields (SCY and KOT). The rest of the subsurface stratigraphy was a similar representation of the three-dimensional (3D) watershed model (Fig. 5b). The land cover was considered as cropland hence the transpiration fitting parameters, LAI, root depth, field capacity, wilting point, oxic, and anoxic limit values for the corresponding crop land were utilized in the model. The observation points were placed at 5 cm, 20 cm, 50 cm, and 100 cm depths. The boundary conditions, initial conditions, forcing climatology data were similar to that of the 3D model. The computational time required by the 1D model to run a daily simulation for a period of 12 years (2010 – 2021) was 5 to 10 minutes using four cores of an Intel® CoreTM i7-8700 processor. This relatively rapid simulation run time facilitated numerous model simulations to analyze the sensitivity of the soil hydraulic parameters and their influence on SM variability of different soil types at deeper depths.

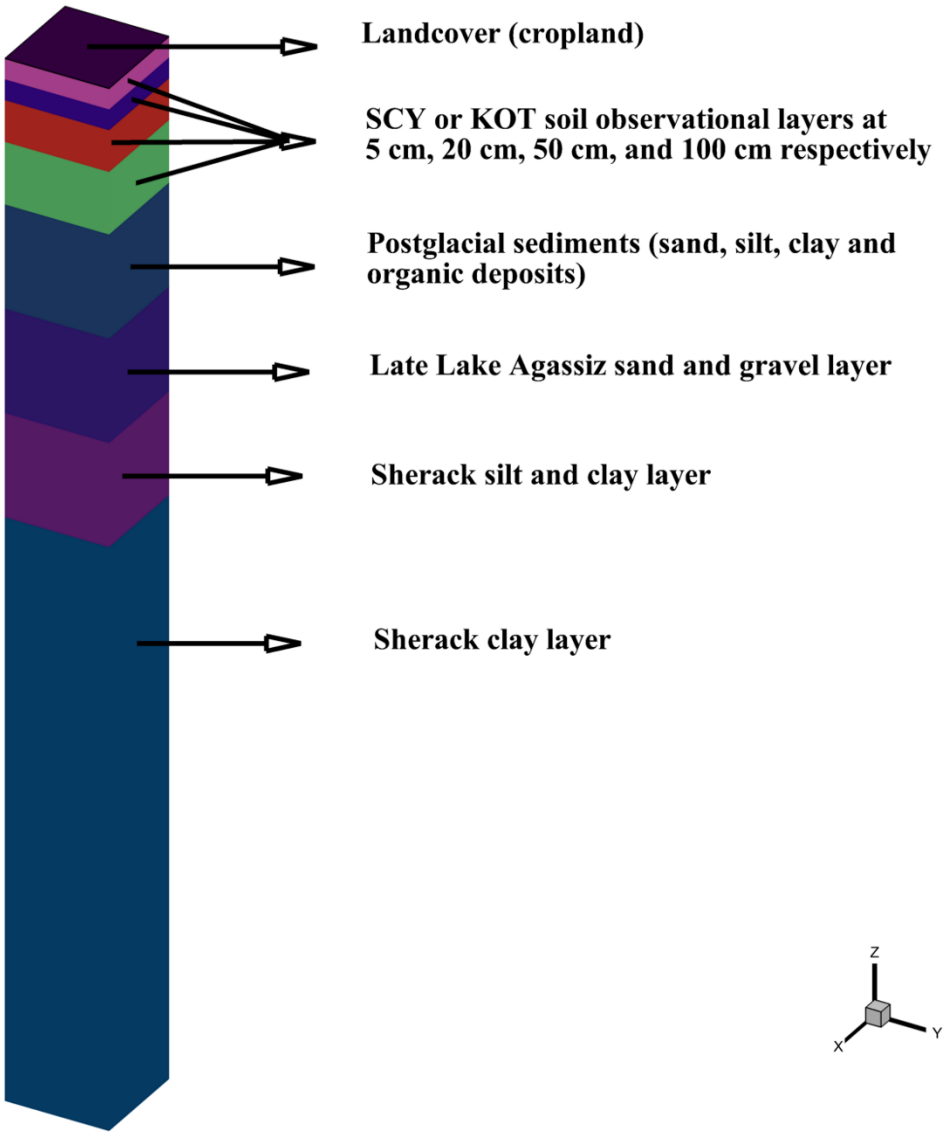

Fig. 6: The 1D model of 1 m x 1 m x 10 m dimensions with surface and subsurface similar to the 3D HGS model.

3.3.10 Automated 1D model calibration using Parameter ESTmation (PEST)

Similar to Martínez García et al. (2014), sensitivity analysis was performed by changing the soil hydraulic parameters and assessing the impact on SM. Changing the parameters had a large impact on SM variability in the top 1 m of the soil. Hence to calibrate the model using the sensitized parameters, Parameter ESTimation (PEST) (Doherty 2010) was integrated with HGS. PEST automates calibration with the model's input and output files and its template files contain the

parameters to change and the results to use for calibration. It also contains a control file which was input with parameter groups from the SCY and KOT soil series at 4 depths individually. The parameter data defined were K, θ_s, θ_r, α, and n. The more observation data available, the more efficiently that PEST can do the calibration. Hence, 1527 SCY measured SM values from RISMA 5 and 1115 KOT measured SM values from RISMA 4 were input as observation data in PEST. The 1D model was subjected to initial manual calibration (optimal values of soil hydraulic parameters) to reduce redundant computational steps. The PEST software calibrated the model by running numerous simulations (the exact number of simulation runs was obtained from the output files). The resultant values of the PEST calibrated parameters were later used to calibrate the 3D model.

3.3.11 Forecasting

Calibration of the model was done using the 2010 – 2020 time period with a spin-up time of 3 years (2010 – 2013). After successful calibration of both the 1D and 3D models, the 2021 growing season daily climatology forcing data (Precipitation + snowmelt and PET) was calculated from the RISMA weather stations for forecasting. The calculated values were appended along with the previously calibrated climate forcing data for the model to simulate a seasonal forecast of daily SM for a specified output time (2021 growing period). The goal was to determine if the model was capable to forecast daily SM with manual addition of input climate forcing data, throughout the catchment in different soil series. Technically, the process of forecasting involves a complete automated prediction of SM values by the model after successful calibration, for a specified future time. However that concept was only partially achieved in this study as the automated process of HGS to obtain the climatological data to calculate SM was fed manually into the model. The model was run to simulate SM for the 2021 growing period and the measured SM values of the 2021

growing season from the RISMA and Sentek stations were compared with the forecasted SM results for both models.

3.3.12 Model performance evaluation

The model performance was evaluated with root mean square error (RMSE), Pearson's correlation coefficient (R), and per cent bias (PBIAS) for simulated vs. observed daily SM values. Generally, in largescale watershed studies, the model output is compared with the measured data with an assumption that all error variance is contained within simulated values and the observed values are error-free. However, Willmott (1981) and the ASCE Task Committee (1993) have shown that measured values are not error-free (e.g. RISMA 5 – the year 2015 measured data has an anomaly). The Pearson's correlation coefficient (R), used to define the correlation between simulated and the observed data, is one of the widely used statistical techniques for model evaluation (Moriasi et al. 2006). Although Santhi et al. (2001) and Van Liew et al. (2003) have provided an acceptable range (values greater than 0.5 are considered acceptable), this statistic is oversensitive to extreme values and insensitive to additive and proportional differences between modelled and measured data (Legates and McCabe 1999). PBIAS was selected because it has the ability to indicate poor model performance involving the calibration of large datasets (Gupta et al. 1999). As recommended by Boyle et al. (2000) and Gupta et al. (1999), the bias measures the average tendency of the simulated values to be consistently larger or smaller than the measured data, and optimizing RMSE during model calibration may reduce error variance.

3.3.13 Simulations

The 1D and 3D models were calibrated for the 2010 – 2020 period and the calibrated models were used to forecast 2021 SM simulation results. It is important to note that the simulated SM values

were available for 2010 – 2021, however, the daily measured SM used to compare the simulated results were available from only mid-June 2013 through August 2021. The RISMA weather stations which provide SM at different depths were installed in 2012 (Ojo et al. 2015) and became operational from June 2013. Hence the statistical analysis between simulated vs. observed was performed only from 2013 – 2020 for calibration and 2021 for forecasting (Table 4). The daily measured SM data for the winter months (November – April) were removed (Table 4) because the dielectric sensors do not provide accurate SM values during winter in frozen soil (Davis and Annan 1977). The forecasted SM was compared with the daily measured SM values from Sentek and RISMA sensors for the 2021 growing period (Table 4) to test SM variability across all soil types and depths by the HGS model. The aforementioned statistical analysis was performed by calculating the volumetric weighted average of the top 100 cm of the soil horizon using the following method:

$$\theta_{V100} = \theta_5 \times 12.5\% + \theta_{20} \times 22.5\% + \theta_{50} \times 40\% + \theta_{100} \times 25\%$$

where θ_{V100} is the volumetric weighted average of top 100 cm soil, θ_5 the soil moisture at 5 cm depth, θ_{20} the soil moisture at 20 cm depth, θ_{50} the soil moisture at 50 cm depth, and θ_{100} the soil moisture at 100 cm depth. The percentage accounts for representative depth of each sensor.

In addition to the top 100 cm, the surface soil moisture of the top 10 cm of the soil profile was also calculated for comparison to the SM values of the 5 cm sensor. The HGS model values for each day were compared to the measured daily SM data, which were also averages of an entire day.

Table 4: The comparative assumptions made for the models.

Model type	Location	Soil type	Calibration period[1]	Forecasting period (2021)
3D	RISMA 4	KOT	2013 – 2020[2]	April - August
	RISMA 5	SCY	2013 – 2020	April - August
	Sentek Sand	WWC	-	June - August
	Sentek Clay	SCY	-	June - August
1D	RISMA 4	KOT	2013 – 2020	April - August
	RISMA 5	SCY	2013 – 2020	April - August

[1]The observed data of the months from November to April were neglected since the instruments cannot distinguish between liquid and frozen soil water content

[2]Measured soil moisture during April is unavailable for a minimum of the first 2 – 3 weeks since the soil is frozen and there was literally "no data" in the weather stations. Hence the April month was neglected for measured data except 2017, 2020, and 2021 where data was available.

3.3.14 2010 – 2021 Climatology

Annual totals of liquid water (rainfall plus snowmelt) and PET in the Brunkild sub-catchment are shown in Table 5. The highest precipitation plus snowmelt occurred in 2010 and the highest PET was in 2012. PET exceeded rainfall plus snowmelt in all years except 2013. From 2010 through 2014, rainfall plus snowmelt exceeded 500 mm but from 2015 through 2021, it was less than 500

mm (note, that the 2021 amounts are only up to August 31). The annual water deficits (rainfall plus snowmelt minus PET) were particularly high negative amounts in 2017, 2018, 2020 and 2021. Drought-limited crop yields were reported in this area in 2018, 2020 and 2021, which is consistent with the large water deficits that were observed. The combination of both below-average rainfall and snowfall also resulted in no spring flooding from 2018 through 2021. The year 2020 had the smallest annual liquid water input of any other year in the previous decade. PET was relatively consistent for the 2010 – 2021 period with an average of 826 mm.

Table 5: Annual liquid water input (snowmelt + rainfall) and potential evapotranspiration (PET) used to force the model, for the Brunkild sub-catchment.

Year	Precipitation + snowmelt (mm)	PET (mm)
2010	802.4	808.0
2011	530	814.3
2012	504.5	872.7
2013	801.4	786.4
2014	528.7	764.6
2015	472.3	860.3
2016	490.6	808.6
2017	335.4	838.5
2018	308.7	866.3
2019	496.1	822.5
2020	260.1	849.3
2021*	300.8	773.0

* Data calculated till 31st August 2021

3.4 Results

3.4.1 PEST calibration results

The maximum change in values after calibration using PEST was observed in the α and n parameters which influenced the shape of the soil moisture retention curve. The calibrated α values of the clay (SCY) series increased by a minimum of 1.1 (1/m) to a maximum of 1.4 (1/m) at all depths more than the values calculated using Rosetta (Table 6). The calibrated PEST values of n for the sand (KOT) series decreased at all depths but there was no specific pattern observed in clay series. The change in values for θ_r, θ_s, and K were relatively small compared to those obtained directly from Rosetta.

3.4.2 Calibration results for clay

The measured soil moisture (θ_{obs}) fluctuated between 24 – 34 % at 5 cm depth consistently and reached 40 – 42 % only on a couple of occasions during the 2014 – 2016 growing season (May-August). The 1D model simulated values between 14 – 36 % for the same depth and season (Fig. B.2) and the 3D model showed higher variability in simulated soil moisture (θ_{sim}) patterns with values ranging closer to θ_{obs} during the 2014 – 2016 growing season (Fig. 7). The growing season of 2017 – 2020, experienced relatively low SM levels when compared to 2014 – 2016 with values between 12 – 32 %. The 3D model simulated similar values to θ_{obs} at 5 cm during the 2017 – 2020 growing season while the 1D model underestimated the 5 cm $\theta_{obs.}$

The fall periods in 2013 through 2016 all recorded a maximum θ_{obs} of more than 30 % at 5 cm depth (Fig. 7). However, maximum θ_{obs} during August in the 2017 – 2020 period was less than 30 % because of below-normal precipitation and high PET. Late fall precipitation during 2017 - 2019 was high, which increased the fall SM levels in those years (Fig. 7) and was captured more

accurately in the 3D model. The θ_{obs} level were the lowest overall for any year in 2020 at 5 cm depth.

Table 6: Values of soil hydraulic parameters from Rosetta before calibration of the 1D model and after PEST calibration

Soil type	Depth (cm)	θ_r (m^3 / m^3)		θ_s (m^3 / m^3)		K (m/s) *		α (1 / m)		n (-)	
		Rosetta	PEST	Rosetta	PEST	Rosetta	PEST	Rosetta	PEST	Rosetta	PEST
KOT	5	0.051	0.050	0.315	0.29	4.7E-5	1.2E-6	3.07	2.9	2.45	2.25
	20	0.050	0.040	0.35	0.33	3.5E-5	6.0E-5	2.96	2.9	2.21	1.56
	50	0.050	0.050	0.35	0.35	3.8E-5	1.3E-5	2.99	2.9	2.26	1.56
	100	0.056	0.050	0.392	0.40	1.6E-5	1.7E-5	2.61	2.89	1.82	1.5
SCY	5	0.092	0.08	0.402	0.42	1.16E-6	2.19E-6	0.78	1.7	1.39	1.4
	20	0.089	0.1	0.432	0.42	1.89E-6	2.19E-6	0.36	1.75	1.51	1.28
	50	0.103	0.1	0.451	0.42	1.38E-6	2.19E-6	0.41	1.75	1.46	1.7
	100	0.108	0.08	0.462	0.44	1.10E-6	2.19E-6	0.46	1.6	1.44	1.3

* The van Genuchten parameters were converted to m/s from the standard cm/day provided by Rosetta.

The surface SM showed a good fit for the 3D model with Pearson's R and RMSE values of 0.53 and 0.060 respectively (Fig. B.3a) while the 1D model showed fairly decent Pearson's R and RMSE values of 0.46 and 0.070, respectively (Table 7) with the simulated values

underestimating the measured values (Fig. B.3b).

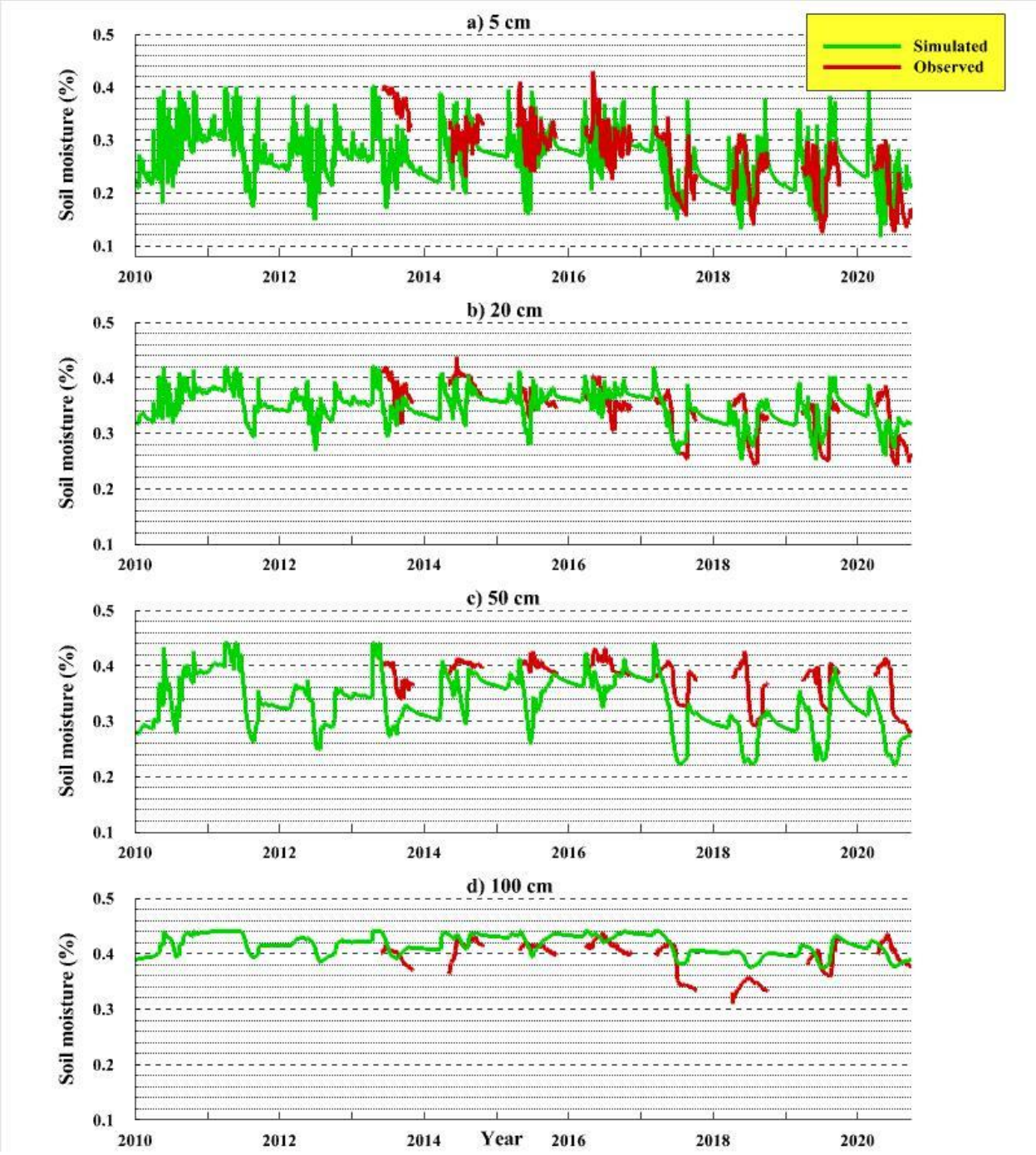

Fig. 7: Time series graph representing calibration (2010 – 2020) results for simulated vs observed soil moisture at a) 5 cm, b) 20 cm, c) 50 cm, and d) 100 cm depth, for the SCY soil series at RISMA 5 using the 3D model.

The θ_{obs} at 20 cm and 50 cm depths remained consistent at 36 – 40 % and 40 – 43 % respectively during the 2013 to 2016 growing season (Fig. 7). The 3D model simulated values similar to θ_{obs} at 20 cm and 50 cm depths in May and June but dropped below 32 % during July and August. The 2013 - 2016 fall seasons showed a rise in θ_{sim} from 32 – 38 % at 20 cm and 50 cm depths (Fig. 7). The 20 cm depth had the best match between θ_{sim} and θ_{obs}. Both the θ_{sim} (3D) and θ_{obs} at 20 cm depth ranged from 25 – 39 %. The θ_{sim} values underestimated θ_{obs}, especially during the 2017 – 2020 period at 50 cm depth (Fig. 7). The θ_{sim} for the 1D model had a good fit for 20 cm and 50 cm throughout all seasons. The 50 cm depth for the 2017 – 2020 period had a better fit for the 1D model as both θ_{sim} and θ_{obs} showed similar results (Fig. B.2).

The 100 cm depth exhibited high θ_{obs} with limited variation throughout the decade. A 41 – 44 % of θ_{obs} and θ_{sim} was observed during the growing season and fall months of 2013 – 2016, when the seasonal decrease of SM during July and August was very minimal at 1 % or 2 %. However, during the 2017 – 2020 period, the θ_{obs} dropped and varied between 32 – 42 % while the θ_{sim} remained consistently higher (38 – 44 %). The 1D model overestimated the measured moisture content and displayed a poor correlation to θ_{obs} at 100 cm depth (Fig. B.2).

The statistical analysis of the top 100 cm (θ_{V100}) of the model exhibited a very good fit for the clay soil series with an R-value of 0.68 and RMSE of 0.040 for the 3D model and a good fit for the 1D model with an R-value of 0.53 and RMSE of 0.033 (Table 7). The positive PBIAS of 5.16 and 13.75 for the 1D and 3D models, respectively indicates that the model was underestimating the θ_{obs}.

Table 7: Statistical analysis results for 1D and 3D model.

		θ_{V100}				Surface soil moisture			
		Clay (SCY)		Sand (KOT)		Clay (SCY)		Sand (KOT)	
Evaluation method	Dimension	Calibration (2010 – 2020)	Forecasting (2021)	Calibration (2010 – 2020)	Forecasting (2021)	Calibration (2010 – 2020)	Forecasting (2021)	Calibration (2010 – 2020)	Forecasting (2021)
R	1D	0.53	0.5	0.41	0.31	0.46	0.52	0.64	0.57
	3D	0.68	0.48	0.49	0.34	0.53	0.50	0.51	0.56
RMSE	1D	0.033	0.030	0.043	0.036	0.070	0.030	0.031	0.021
	3D	0.040	0.024	0.04	0.035	0.060	0.070	0.049	0.030
PBIAS	1D	5.16	-6.20	4.07	-13.00	15.83	-7.03	0.02	-16.07
	3D	13.75	-2.70	1.95	-14.94	28.46	-29.87	24.08	17.47

3.4.3 Calibration results for sand

The sandy (KOT) soil series showed higher variability in SM patterns than SCY. The θ_{sim} and θ_{obs} at 5 cm depth varied between 3 – 28 % through the 2013 – 2015 growing season. The θ_{obs} experienced a temporary periodic rise between 20 – 22% during mid-June due to precipitation in 2014 and 2015 (Fig. 8). The 1D and 3D model θ_{sim} overestimated θ_{obs} and rose to 24 – 28 % in 2015. A steady decline from a maximum of 18 % to less than 10 % θ_{obs} was observed during September to November at 5 cm depth for both modelled and measured data. The growing seasons

of 2017 – 2020 displayed both θ_{sim} and θ_{obs} values between 2 – 15 % which increased to a maximum of 24 % during the fall season. Precipitation during the last week of August in 2016, 2018, and 2019 increased both θ_{sim} and θ_{obs} levels for the subsequent year's spring season. However, the 1D and 3D models overestimated the measured values at the surface during the growing season. The statistical analysis of surface SM showed a good fit between θ_{sim} and θ_{obs} with an R-value of 0.64 for the 1D model and 0.51 for the 3D model (Table 7). The 1D model performed relatively better than the 3D model only for surface SM with Pearson's R-value of 0.64, RMSE of 0.031, and PBAIS producing an optimal value of 0.02 (Figs. B.4, B.5a, and B.5b)

The growing season of 2013 – 2015 saw sharp declines in θ_{obs} at 20 cm and 50 cm depths while θ_{sim} by both the models remained consistent with less variation in their patterns (Figs. 8 and B.4). The θ_{sim} during the growing season of 2013 – 2015 measured between 14 – 22 % at 20 cm and 18 – 33 % at 50 cm for both models. The θ_{obs} during the 2017 – 2020 growing season decreased from approximately 38 % to below 20 % during July at 50 cm depth. However, the θ_{sim} declined from 28 % to 9 % at 20 cm and a maximum of 24 % to 16 % at 50 cm depth.

The θ_{obs} was 38 – 40 % during the growing season of 2013 – 2015 at 100 cm depth. The seasonal decline during July and August months dropped θ_{obs} to 31 %. During the 2017 – 2020 period, the θ_{obs} was lower and varied between 22 – 40 % while the 1D and 3D θ_{sim} values were 32 – 42 % consistently throughout the decade. The 100 cm depth showed a poor correlation between θ_{sim} and θ_{obs}.

The statistical analysis of the top 100 cm (θ_{V100}) of the model showed a reasonably good fit from the 3D model with an R-value of 0.49 and RMSE of 0.04 (Table 7) while the 1D model underestimated the measured values and showed lower correlation with an R-value of 0.41 and RMSE of 0.043.

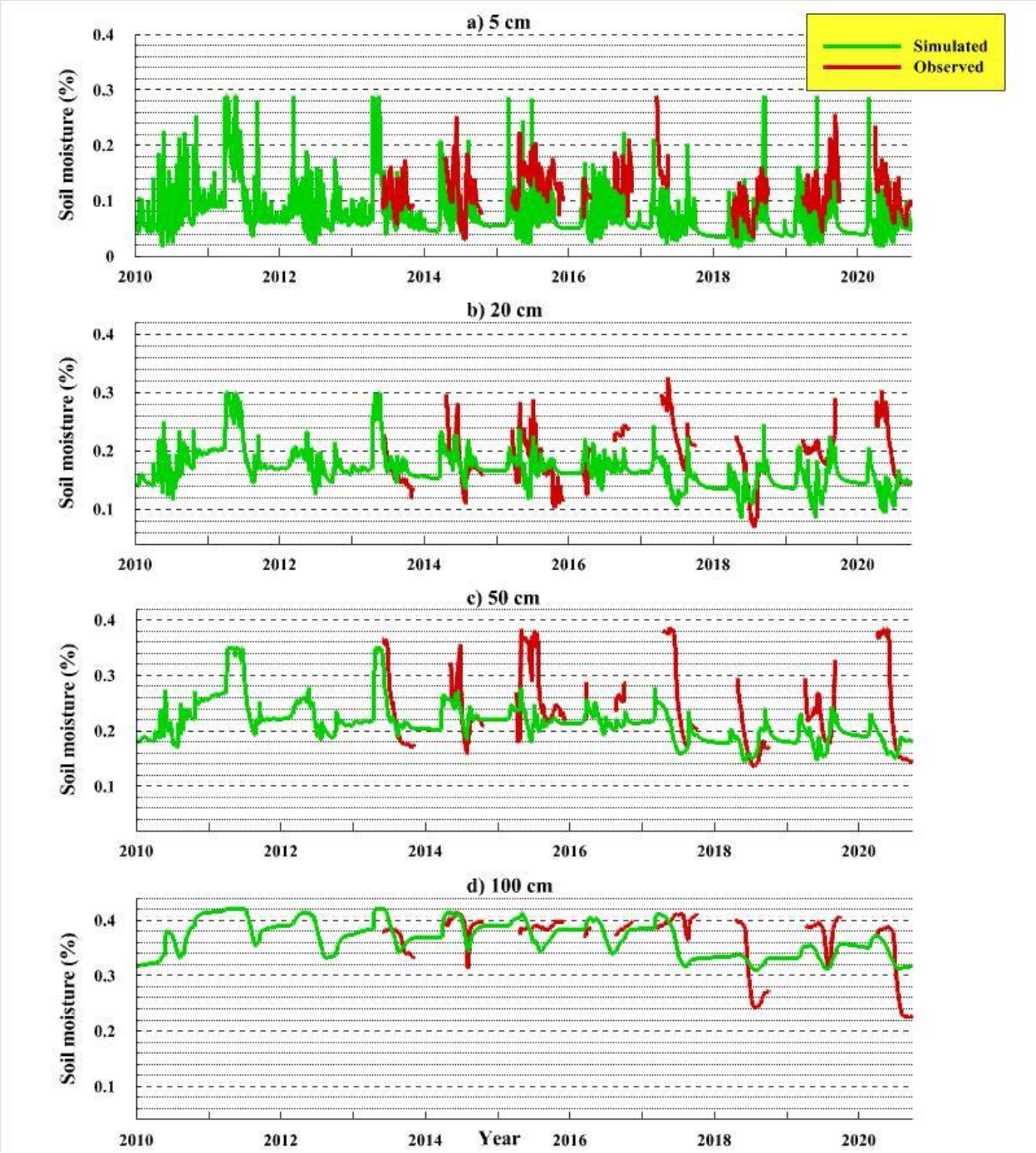

Fig. 8: Time series graph representing calibration (2010 – 2020) results for simulated vs observed soil moisture at a) 5 cm, b) 20 cm, c) 50 cm, and d) 100 cm depth, for KOT soil series at RISMA 4 using the 3D model.

3.4.4 Forecasting results for sand and clay at RISMA and Sentek observational fields

Both 1D and 3D calibrated models were used to forecast SM for the 2021 growing season. Because of the early growing season dryness, the θ_{obs} for the clay soil (SCY) at 20 cm, 50 cm, and 100 cm was low at the beginning and increased as the growing season progressed. Both models overestimated the θ_{obs} at 5 cm and 20 cm depths and underestimated the θ_{obs} at 50 cm and 100 cm depths (Figs. B.6 and B.7). For 2021 overall, both the models produced fairly good forecasting statistical results with an average R-value of 0.5 (Table 7) for both surface and the θ_{V100}. The θ_{V100} comparison yielded good results with RMSE values of 0.030 and 0.024 and PBIAS values of -6.2 and -2.7 for 1D and 3D models, respectively (Table 7).

Contrary to SCY, the KOT soil series at RISMA 4 produced weak forecasting results for the overall top 100 cm depth. As expected, the surface θ_{obs} were low during the 2021 growing season with values down to 1 – 2 % during July and August. The surface θ_{sim} showed good results in both models with Pearson's R of 0.57 and 0.56 and RMSE values of 0.021 and 0.030 in the 1D and 3D models, respectively (Figs. B.6 and B.7). The forecasting results for the KOT series θ_{sim} at 50 cm and 100 cm depth overestimated θ_{obs}. The θ_{obs} values fluctuated between 10 – 20 % at 50 cm and consistently less than 30 % at 100 cm depth throughout the growing season.

The Sentek sensors had the least number of data points for comparison with the forecasted data as they were installed in the fields for less than three months (71 days). The θ_{obs} at Sentek clay displayed a range similar to RISMA 5 since both the fields have the same SCY soil series. However, the θ_{obs} for Sentek clay at 50 cm and 100 cm depths increased above 50 % during the growing season while the θ_{sim} reached a maximum of only 40 – 42 %. The Sentek clay field θ_{sim} showed a good correlation with θ_{obs} for the surface with an R-value of 0.71 and the overall top 100 cm soil profile volumetric average measurement with an R-value of 0.70 (Table 8). Sentek sand

was in the sandy WWC soil series and showed low θ_{obs} during June – August (Fig. B.8). The θ_{obs} and θ_{sim} at 5 cm ranged between 2 – 4 % during June – August, while the 20 and 50 cm depth range was less than 20 %, indicating drought conditions. The θ_{sim} at overall depth underestimated the θ_{obs} by a big margin. The forecast results for Sentek sand at the surface produced the best match CAwith optimal values of R, RMSE, and PBIAS (0.81, 0.011, and -5.01). On the other hand, the overall volumetric average for the top 100 cm for Sentek sand was a weak match with the θ_{obs} and underestimated the θ_{obs} values (Table 8).

Table 8: Statistical analysis of forecasted results compared with measured soil moisture value at Sentek stations.

	θ_{V100}		Surface soil moisture	
	Clay (SCY)	Sand (WWC)	Clay (SCY)	Sand (WWC)
R	0.70	0.31	0.71	0.81
RMSE	0.02	0.085	0.052	0.011
PBIAS	-1.69	40.41	-20.82	-5.01

3.4.5 Comparison of results

The statistical results of surface SM measurements (Table 7) showed the ability of the model to replicate SM at single point locations. The sand (KOT) series in the 1D model showed an excellent match between simulated and observed values at the surface (Table 7) while sand 3D and clay 1D and 3D results produced a good correlation for the surface during calibration and forecasting (Tables 7 and 8). However, for the lower soil depths, clay 20 cm showed the best match during calibration and forecasting (Figs. 7 and B.6) for the 3D model while 20 cm and 50 cm depth of 1D model showed the best match (Figs. B.4 and B.7).

The greatest difference between θ_{obs} and θ_{sim} was observed at 50 cm depth for both SCY and KOT soil series. The growing season SM increased or stayed consistent during May and June while July and August saw the largest decrease in θ_{obs} at all depths (Figs. 7 and 8). However, the 50 cm θ_{obs} at RISMA 5 were consistently high during the 2013 – 2016 growing season while the θ_{sim} showed a pattern of declining SM during the 2013 – 2016 growing season (Fig. 7). The 50 cm θ_{obs} at RISMA 4 had one anomaly during 2015 (Fig. 8). Although there is no official record from Manitoba agriculture for any reported issues, the seasonal pattern was different from the rest. June 16^{th} – 18^{th} (2015) recorded 4.4 mm precipitation, the 5 cm, 20 cm, and 100 cm had its SM increased by 3 – 6 % however the 50 cm depth recorded an increase from 17 % to 39 % in one day. The θ_{obs} of 2015 could not be neglected from the calculation as KOT with 1115 data points had approximately 400 data points less than SCY with 1527 for comparing θ_{sim} and θ_{obs}. The main reason was that the 2016 year had its entire growing season (Mid-April to Mid-September) record missing from the database. Although both the models simulated the seasonal SM patterns, the 20 cm and 50 cm forecasts for the KOT series underestimated the measured values during calibration and forecasting. However, the 3D model was able to reproduce the decrease in SM patterns in KOT, especially during the 2017 – 2021 period. Because similar seasonal trends in SM were being reproduced by the 3D model, it showed a reasonably good fit with an R value of 0.49 while the 1D model showed a poor fit for the θ_{V100} of the soil profile.

3.5. Discussion

The physically-based 3D model employed in this study was able to replicate the extremes in hydrologic behavior of the Brunkild sub-catchment over the 2010 – 2020 time interval and it also forecasted daily SM values reasonably well for the 2021 growing season. It included years that had spring flooding (2013 - 14, and 2017), extreme drought years of 2020, and 2021 and years that had abundant late fall precipitation (2019). Despite the structural complexity of the fully-integrated model for the Brunkild sub-catchment, the model exhibited creditable performance when simulating and forecasting SM at different depths in multiple soil series growing different crops during each growing season.

The Brunkild sub-catchment underwent seasonal transitions between frozen and thawed states which were observed to be variable and were modified spatially and temporally under the changing climate. The snowmelt usually occurred during the latter half of March and several days throughout April from 2011 to 2020 (no data for 2010) excluding 2021 when the snow melted during the last week of February and early March. The SM freeze-up during fall can be highly variable for different soil types as a certain volume of water remained unfrozen due to capillary and adsorptive forces (Pardo Lara et al. 2021). The soil freeze-up starts at the surface layer (5 cm) and goes further to 100 cm depth eventually. Due to soil freeze-up, it was noted that the dielectric sensors at the weather stations stopped providing data for both sand and clay at the same time. It occurred during November for most years in the past decade except 2015 and 2016 when the soil froze in mid-December. During early spring, the sandy soil series thawed a couple of weeks before the clay on a few occasions. However, there was no consistent pattern of θ_{obs} data in both soil series to check the exact thawing period. Using proper forcing data and initial conditions, the HGS model was able to simulate SM during the spring season by considering the fall moisture data from

the previous years. The peaks in simulated SM in the 3D model (Figs. 7, and 8) during wet April months were the result of high-water content due to high snow accumulation during the winter.

The year 2010 had high SM because of abundant rain during all seasons (early spring, growing season, and fall), which resulted in excess SM (Crop report 2010) and decreased crop yields. This situation was replicated by the 3D model for both sand and clay soil series at all the depths while the 1D model underestimated the θ_{obs} values at deeper depths in 2010. Due to the unavailability of θ_{obs} data for this period, a quantitative assessment could not be made. But it can safely be assumed that the 3D model with successful calibration reproduced the pattern better because it showed high water availability throughout the season which matched the pattern of the forcing data. A pattern of spring flooding because of heavy snow accumulation, followed by a cold dry spring and consistently moist growing season, and finally with September frost was noticed during the years 2011, 2013, and 2014. In contrast to that, a pattern of cold dry spring with no spring flooding, below-normal growing season precipitation and late fall precipitation was observed in 2015, 2016, 2018, and 2019. A drastic change in climate patterns was observed in 2020 and 2021. The conditions in 2020 started with high SM because of abundant 2019 fall precipitation however, the low snow accumulation, dry growing season and below normal fall precipitation resulted in severe drought which was eventually reflected in the 2021 forecasted SM. The 50 cm and 100 cm depths consistently produced high θ_{obs} because of the shallow groundwater table in the study area during the growing period. It can be because the water content in the deep soil layers maintains an upward vertical SM gradient. While the soil layers at the top are heavily influenced by evapotranspiration (ET) the lower layers are replenished by groundwater. In addition to the influence of groundwater, the hydraulic conductivity of subsurface layers below 1 m impacted SM variability at 100 cm depth which was observed during calibration. However, the 1D model did not reproduce the SM pattern

at deep layers despite proper calibration and showed a poor correlation. Considering only the vertical distribution, the main watershed model was an approximate replica of the surficial geology level with coarse discretization, which could be a factor affecting the SM distribution at deeper depth in the 1D model. A detailed assessment of the influence of groundwater could not be made due unavailability of groundwater data because the monitoring well at Brunkild stopped functioning. Groundwater data from neighboring catchments proved to be hydrogeologically irrelevant for the Brunkild sub-catchment.

The 50 and 100 cm depth during 2017 – 2021 indicated the influence of evapotranspiration during July and August when the temperature was high and the crops reached full canopy cover. The low soil water content at 5 cm and 20 cm indicated a water deficit at the surface, thus the crops were utilizing the water from deeper depths. Soil properties, and more specifically soil hydraulic properties, often have the largest influence on SM variability (Martínez García et al. 2014), which was supported by the results in this study during the sensitivity analysis. Changes in the α, n, and K values had the largest influence on the soil moisture retention curve. The residual water content (θ_r) and the saturated water content (θ_s) controlled the maximum and minimum range of SM values at a particular depth. The RISMA 5 θ_{obs} values were equal to θ_{sim} proving the influence of θ_s values which were computed by PEST during calibration. The parameters α and n controlled the steepness of the soil moisture retention curve in the model while the K showed the least influence among the van Genuchten parameters. Decreasing the pore size distribution value at a specific depth increased the overall SM at that depth but no specific pattern was observed while changing the inverse of air entry suction. However, it was observed during sensitivity analysis that the α and n parameters influence the θ_{sim} by a large margin.

The shallow geology of the Brunkild sub-catchment had an important interflow component with subsurface water (moisture at 20 – 100 cm) draining from the sandy soils on the west towards the east along the texture divide which in turn produced high SM content at the surface in clayey soils present at the sand-clay interface. The sharp contrast in soil texture from west to east as well as the fact that the sandy soils are underlain by heavy clay along the texture boundary provides conditions that are conducive to interflow. The high SM content at the surface at the RISMA 5 observational field was mainly controlled by lateral and vertical flow processes and the spatial distribution of soil porosity. According to Kim and Mohanty (2016), the anisotropy in hydraulic conductivity influences the lateral subsurface flow process. At Brunkild, the effects of anisotropy on SM were not noticed when SM was low but it had an effect under wet SM conditions. This happened because the SM is greater than the field capacity. This enhances the lateral flux of water and leads to high water content. This concept can only be captured by the HGS 3D model which models flow in 3 dimensions while the 1D model only models vertical flow and cannot take lateral flow into account. Vereecken et al. (2008) explained that cases involving analysis of soil profile SM in humid and semi-arid landscapes where lateral flow is an important contribution for runoff, the use of a 1D model might not provide accurate model results. Hence, despite the decent 1D model results at the surface level for both soil series, inappropriate selection of model dimension might corrupt the soil hydraulic parameter estimates and might affect the model predictions.

The overall underestimation of the measured values by the calibrated model can be due to several limitations. This includes the degree of error in the forcing data that were collected from multiple weather stations. The daily climate forcing data used the average of precipitation data from neighboring weather stations (Table 3), which also assisted to fill missing data (Kusiak et al. 2017). The model forcing data for the entire Brunkild sub-catchment may not be representative of water

input to a specific field. For example, RISMA 4 received 24 mm precipitation on 26th June 2014 while RISMA 5 received only 14 mm of precipitation on the same day. The resultant mean precipitation of 19 mm was used as forcing data for the model for that specific day. The RISMA 5 Hydra probe sensors measured the rise in SM in response to the precipitation received at RISMA 5 specifically while RISMA 4 measured SM response to the precipitation it received. However, the model was forced with 19 mm precipitation on 26th June 2014 at both RISMA 4 & 5. The results will show that there was precipitation and an increase in SM across all the depths, however, the values will be over or underestimated according to the precipitation and PET at each specific field. A similar principle can be applied to PET forcing data as well. This is one of the prime reasons for the difference in θ_{obs} and θ_{sim} at individual observation points. In addition, the SNODAS and MODIS model outputs that were used as forcing data are always accompanied with an error percentage within them, hence these forcing data are not precise. During the drought years (2019, 2020 and 2021) it was reported that farmers sowed their seeds at the subsurface (10 – 15 cm below the soil instead of 5 cm) as the topsoil was extremely dry. Low snow resulted in low snowmelt and low surface SM for the seeds to germinate. The low SM levels are reproduced and forecasted in the model but the change in seeding depth alters the measure of evapotranspiration depth from the cropland landcover that was a constant for the model and was not considered to be time-varying. The seeds sowed at the subsurface utilize the subsurface moisture to germinate instead of the early spring precipitation which might affect the model results. However, during sensitivity analysis, it was observed that change in evaporation depth had little influence on the change in SM over a large scale. An advantage of the structurally complex large-scale agriculture watershed model is that it incorporates a physics-based evaluation of the natural system, making many of its parameters physically constrained (Frey et al. 2021). However, the computational time

to run a simulation can be long relative to a simpler model. The 3D Brunkild HGS model in this study required approximately 5 days for completion of continuous daily temporal resolution simulations of the 2010 – 2021 time interval when using four cores of an Intel® CoreTM i7-8700 processor.

Mazrooei et al. (2020) described forecasting SM at surface level using satellite sensors and stated that the ability to forecast SM has not been carried out over larger domains. However, this study has shown credible results with forecasting daily SM levels over deeper depths using the HGS model over a mesoscale catchment. Forecasting accurate SM can support planning and management of water resources and can significantly assist decision-making for agricultural management. In this research, manual addition of climate forcing data into the HGS model can be considered the first step in determining the model forecasting capabilities. Integrating HGS with modelled predictions of forcing climatological data (precipitation, snowmelt and PET) data such as the Meteorological Service of Canada (MSC) Global Ensemble Prediction System (GEPS) (https://weather.gc.ca/grib/grib2_ens_geps_e.html) would assist in the real-time production and automation of the SM forecast process. If HGS was capable of accessing the forecasted climate forcing data, it could simulate SM over the forecast period. Forecasting SM at deeper depths assists farmers with optimizing irrigation application both increasing crop yield and minimizing redundant irrigation costs. Forecasting viability, which was an important objective of this research, produced good results for clayey soils at all depths while the sand soil produced the best results at the surface. The statistical analysis of clay soil at both RISMA and Sentek observational fields showed better forecasting results. Hence HGS is capable of being developed as a forecasting tool for deeper depths in catchments dominated by clay soils. Agriculture and Agri-Food Canada (2021) declared 2021 as an agriculture disaster due to low yields and extremely low SM content

and 2010 experienced abundant precipitation and high SM which also resulted in low yields. The Brunkild HGS model evaluation experienced both extremes in little more than one decade. Despite the challenges, the model was able to reproduce credible statistical results across the sub-catchment. According to Refsgaard (1997), the model created for a specific area can be considered good if it is capable of creating sufficiently accurate simulations for its intended purpose. However, the definition of "sufficiently accurate" can vary based on project goals.

3.6 Conclusion

This study constructed physically-based groundwater-surface water 1D and 3D HGS models for an agriculturally dominated watershed to test the modeled accuracy of SM through the root zone of soil in a cold climate. The calibrated models were able to display good results for clay soils and reasonable results for sandy soils. The calibrated models provided answers to several scientific questions related to catchment level spatial and temporal heterogeneity of SM, extent of the influence of soil hydraulic parameters in soil water retention curves, and lateral movement of water and its effect on SM in different soil types. It was concluded that the 3D model slightly underestimated the measured SM values due to a few limitations previously discussed. As a result of successful calibration, the model was able to forecast reasonably accurate SM for the 2021 growing season in comparison to measured SM at four observation points with contrasting soils within the Brunkild sub-catchment. It was observed that both calibrated and forecasted SM in clay displayed good correlation at all depths while the sand series showed good correlation at the surface and weaker correlation at the deeper depths.

Further study on model development and soil hydraulic parameters to simulate SM in places dominated by sandy soil can be a scope for future work as well as developing a complete tool to automate SM forecasting using HGS. A comparison of SM variability at the catchment scale using

two contrasting spatial resolutions (1: 1 million and 1: 20,000) of soil survey data is currently under consideration.

Chapter 4 – Conclusion

The study provided a comprehensive analysis of the SM variations in the hydrologically challenging conditions of the Red River Valley. The simulated SM results showed higher spatial and temporal variability for coarse-textured soil series than that of fine-textured soil. Larger variability in SM was observed at the shallow depth than the deeper depth in both soil series. It was also concluded that soil hydraulic parameters had the largest impact in influencing the soil moisture variation. The creation of the 1D model proved to be useful for sensitivity analysis however it was not able to capture the lateral flow process that was captured by the 3D model. The study proved that with proper input variables and high computational power of the work machine, the model will be able to forecast SM with good results for an area dominated by clay soils at deeper depths while sand soil series despite a weak correlation will be able to follow the spatiotemporal pattern of the measured soil moisture from weather stations. Techniques to measure SM like remote sensing, and statistical models produce good surface SM measurements. It is the same in the case of HGS, however, good SM prediction at deeper layers gives physically-based models like HGS an advantage.

Chapter 5 – Future work

- A comparison of SM variability at the catchment scale using two contrasting spatial resolutions (1: 1 million and 1: 20,000) of soil survey data is currently under consideration.

- Because of relatively good results for a mesoscale catchment, a model comprising a study area covering the entire Red River Valley could be built to analyze the soil moisture variation.
- The simulated groundwater measurements and stream flow could be calculated and analyzed with measured values to strengthen the model performance.
- New techniques to improve the time-stepping process could be considered in future to decrease the computation time of individual simulation runs.
- Comparative analysis between other SM prediction techniques like data assimilation algorithms and data-driven methods could be compared with the HGS modelled forecasted results to determine the advantages and disadvantages of using a specific technique.
- Further study on model development and soil hydraulic parameters to simulate SM in places dominated by soil other than clay (sandy, silt etc.) can be a scope for future work.
- Building a complete SM forecasting tool by integrating HGS with external weather predictions can be a scope for future work.

References

Agriculture and Agri-Food Canada. 2021. Canadian Drought Monitor Conditions report.

Alakukku, L., Weisskopf, P., Chamen, W.C.T., Tijink, F.G.J., van der Linden, J.P., Pires, S., Sommer, C., and Spoor, G. 2003. Prevention strategies for field traffic-induced subsoil compaction: a review. Soil & tillage research, **73**(1-2): 145-160. doi:10.1016/S0167-1987(03)00107-7.

An, Y., Lu, W., and Yan, X. 2018. A surrogate-based simulation–optimization approach application to parameters' identification for the HydroGeoSphere model. Environmental Earth Sciences, **77**(17). doi:10.1007/s12665-018-7806-7.

ASCE Task Committee. 1993. Criteria for Evaluation of Watershed Models. Journal of irrigation and drainage engineering, **119**(3): 429-442. doi:10.1061/(ASCE)0733-9437(1993)119:3(429).

Berg, S.J., and Sudicky, E.A. 2019. Toward Large-Scale Integrated Surface and Subsurface Modeling. Ground Water, **57**(1): 1-2. doi:10.1111/gwat.12844.

Bhuiyan, H.A.K.M., McNairn, H., Powers, J., Friesen, M., Pacheco, A., Jackson, T.J., Cosh, M.H., Colliander, A., Berg, A., Rowlandson, T., Bullock, P., and Magagi, R. 2018. Assessing SMAP Soil Moisture Scaling and Retrieval in the Carman (Canada) Study Site. Vadose Zone Journal, **17**(1): 180132. doi:10.2136/vzj2018.07.0132.

Blume, T., Zehe, E., and Bronstert, A. 2009. Use of soil moisture dynamics and patterns at different spatio-temporal scales for the investigation of subsurface flow processes. Hydrology and Earth System Sciences, **13**: 1215-1234.

Boyle, D.P., Gupta, H.V., and Sorooshian, S. 2000. Toward improved calibration of hydrologic models: Combining the strengths of manual and automatic methods. Water Resources Research, **36**(12): 3663-3674. doi:10.1029/2000wr900207.

Brunner, P., and Simmons, C.T. 2012. HydroGeoSphere: A Fully Integrated, Physically Based Hydrological Model. Ground Water, **50**(2): 170-176. doi:10.1111/j.1745-6584.2011.00882.x.

Canadell, J., Jackson, R.B., Ehleringer, J.R., Mooney, H.A., Sala, O.E., and Schulze, E.D. 1996. Maximum Rooting Depth of Vegetation Types at the Global Scale. Oecologia, **108**(4): 583-595.

Cantón, Y., Solé-Benet, A., and Domingo, F. 2004. Temporal and spatial patterns of soil moisture in semiarid badlands of SE Spain. Journal of Hydrology, **285**(1): 199-214. doi:https://doi.org/10.1016/j.jhydrol.2003.08.018.

Chaparro, D., Vall-llossera, M., Adrinano Camps, M.P., Rudiger, C., and Riera-Tatche, R. 2016. Predicting the Extent of Wildfires Using Remotely Sensed Soil Moisture and Temperature Trends. IEEE Journal of Selected Topics in Applied Earth Observations and Remote Sensing, **9**(6).

Chen, Y., Marek, G.W., Marek, T.H., Moorhead, J.E., Heflin, K.R., Brauer, D.K., Gowda, P.H., and Srinivasan, R. 2018. Assessment of Alternative Agricultural Land Use Options for Extending the Availability of the Ogallala Aquifer in the Northern High Plains of Texas. Hydrology, **5**(4): 53. Available from https://www.mdpi.com/2306-5338/5/4/53 [accessed.

Chifflard, P., Kranl, J., Strassen, G.z., and Zepp, H. 2018. The significance of soil moisture in forecasting characteristics of flood events. A statistical analysis in two nested catchments. Journal of Hydrology and Hydromechanics, **66**(1): 1-11. doi:10.1515/johh-2017-0037.

Cho, E., Choi, M., and Wagner, W. 2015. An assessment of remotely sensed surface and root zone soil moisture through active and passive sensors in northeast Asia. Remote Sensing of Environment, **160**: 166-179. doi:10.1016/j.rse.2015.01.013.

Cornelissen, T., Diekkrüger, B., and Bogena, H. 2013. Using HydroGeoSphere in a Forested Catchment: How does Spatial Resolution Influence the Simulation of Spatio-temporal Soil Moisture Variability? Procedia Environmental Sciences, **19**: 198-207. doi:10.1016/j.proenv.2013.06.022.

Cornelissen, T., Diekkrüger, B., and Bogena, H.R. 2014. Significance of scale and lower boundary condition in the 3D simulation of hydrological processes and soil moisture variability in a forested headwater catchment. Journal of Hydrology, **516**: 140-153. doi:10.1016/j.jhydrol.2014.01.060.

Cornelissen, T., Diekkrüger, B., and Bogena, H. 2016. Using High-Resolution Data to Test Parameter Sensitivity of the Distributed Hydrological Model HydroGeoSphere. Water, **8**(5): 202. doi:10.3390/w8050202.

Crop report. 2010. Manitoba Agriculture, Food and Rural Initiatives GO Teams & Crop Knowledge Centre. (Issue 26). doi:http://www.gov.mb.ca/agriculture/crops/seasonalreports.html

Crop Report Summary, C.r. 2021. Manitoba Agriculture & Resource Development. Primary Agriculture Branch. doi:https://www.gov.mb.ca/agriculture/crops/seasonal-reports/crop-report-archive/.

Davis, J.L., and Annan, A.P. 1977. Electromagnetic Detection of Soil Moisture: Progress Report I. Canadian Journal of Remote Sensing, **3**(1): 76-86. doi:10.1080/07038992.1977.10854959.

Doherty, J. 2010. PEST, Model-Independent Parameter Estimation—User Manual. 5th Edition, with Slight Additions, Watermark Numerical Computing, Brisbane.

Dorigo, W.A., Gruber, A., De Jeu, R.A.M., Wagner, W., Stacke, T., Loew, A., Albergel, C., Brocca, L., Chung, D., Parinussa, R.M., and Kidd, R. 2015. Evaluation of the ESA CCI soil moisture product using ground-based observations. Remote Sensing of Environment, **162**: 380-395. doi:10.1016/j.rse.2014.07.023.

Fatichi, S., Vivoni, E.R., Ogden, F.L., Ivanov, V.Y., Mirus, B., Gochis, D., Downer, C.W., Camporese, M., Davison, J.H., Ebel, B., Jones, N., Kim, J., Mascaro, G., Niswonger, R., Restrepo, P., Rigon, R., Shen, C., Sulis, M., and Tarboton, D. 2016. An overview of current applications, challenges, and future trends in distributed process-based models in hydrology. Journal of Hydrology, **537**: 45-60. doi:10.1016/j.jhydrol.2016.03.026.

Fisette, T., Rollin, P., Aly, Z., Campbell, L., Daneshfar, B., Filyer, P., Smith, A., Davidson, A., Shang, J., and I., J. 2013. AAFC annual crop inventory, . 2013 Second International Conference on Agro-Geoinformatics (Agro-Geoinformatics),: 270-274. Available from doi: 10.1109/Argo-Geoinformatics.2013.6621920. [accessed.

Freeze, R.A., and Cherry, J.A. 1979. Groundwater.

Frey, S.K., Miller, K., Khader, O., Taylor, A., Morrison, D., Xu, X., Berg, S.J., Hwang, H.T., Sudicky, E.A., and Lapen, D.R. 2021. Evaluating landscape influences on hydrologic behavior with a fully-integrated groundwater – surface water model. Journal of Hydrology, **602**: 126758. doi:10.1016/j.jhydrol.2021.126758.

Gao, X., Rajendran, N., Tenuta, M., Dunmola, A., and Burton, D.L. 2014. Greenhouse Gas Accumulation in the Soil Profile is not Always Related to Surface Emissions in a Prairie Pothole Agricultural Landscape. Soil Science Society of America Journal, **78**(3): 805-817. doi:10.2136/sssaj2013.05.0157.

Goderniaux, P., Brouyère, S., Fowler, H.J., Blenkinsop, S., Therrien, R., Orban, P., and Dassargues, A. 2009. Large scale surface–subsurface hydrological model to assess climate change impacts on groundwater reserves. Journal of Hydrology, **373**(1-2): 122-138. doi:10.1016/j.jhydrol.2009.04.017.

Grisak, G.E., and Cherry, J.A. 1975. Hydrologic Characteristics and Response of Fractured Till and Clay Confining a Shallow Aquifer. Canadian Geotechnical Journal, **12**(1): 23-43. doi:10.1139/t75-003.

Grisak, G.E., and Jackson, R.E. 1978. An appraisal of the hydrogeological processes involved in shallow subsurface radioactive waste management in Canadian terrain. Department of the Environment.

Gupta, H.V., Sorooshian, S., and Yapo, P.O. 1999. Status of Automatic Calibration for Hydrologic Models: Comparison with Multilevel Expert Calibration. Journal of hydrologic engineering, **4**(2): 135-143. doi:10.1061/(ASCE)1084-0699(1999)4:2(135).

Hargreaves, G.H., and Samani, Z.A. 1985. Reference Crop Evapotranspiration from Temperature. Applied Engineering in Agriculture, **1**(2): 96-99. doi:10.13031/2013.26773.

Hawley, M.E., Jackson, T.J., and McCuen, R.H. 1983. Surface soil moisture variation on small agricultural watersheds. Journal of Hydrology, **62**(1): 179-200. doi:https://doi.org/10.1016/0022-1694(83)90102-6.

Hébrard, O., Voltz, M., Andrieux, P., and Moussa, R. 2006. Spatio-temporal distribution of soil surface moisture in a heterogeneously farmed Mediterranean catchment. Journal of Hydrology, **329**(1): 110-121. doi:https://doi.org/10.1016/j.jhydrol.2006.02.012.

Herbst, M., and Diekkrüger, B. 2003. Modelling the spatial variability of soil moisture in a micro-scale catchment and comparison with field data using geostatistics. Physics and Chemistry of the Earth, Parts A/B/C, **28**(6-7): 239-245. doi:10.1016/s1474-7065(03)00033-0.

HydroAlgorithmics. 2016. AlgoMesh User Guide. HydroAlgorithmics Pty Ltd.

Kim, J., and Mohanty, B.P. 2016. Influence of lateral subsurface flow and connectivity on soil water storage in land surface modeling. Journal of Geophysical Research: Atmospheres, **121**: 704-721. doi:10.1002/2015JD024067.

Kristensen, K.J., and Jensen, S.E. 1975. A model for estimating actual evaporation from potential evapotranspiration. Nordic Hydrology, **6**: 170-188.

Krzeminska, D.M., Steele-Dunne, S.C., Bogaard, T.A., Rutten, M.M., Sailhac, P., and Geraud, Y. 2012. High-resolution temperature observations to monitor soil thermal properties as a proxy for soil

moisture condition in clay-shale landslide. Hydrological Processes, **26**(14): 2143-2156. doi:10.1002/hyp.7980.

Kuang, W., Gao, X., Tenuta, M., Gui, D., and Zeng, F. 2019. Relationship between soil profile accumulation and surface emission of N2O: effects of soil moisture and fertilizer nitrogen. Biology and Fertility of Soils, **55**(2): 97-107. doi:10.1007/s00374-018-01337-4.

Kusiak, A., Rezazadeh-Joudi, A., and Sattari, M.-T. 2017. Assessment of different methods for estimation of missing data in precipitation studies. Hydrology Research, **48**(4): 1032-1044. doi:10.2166/nh.2016.364.

Lee, S., Yeo, I.Y., Lang, M.W., Sadeghi, A.M., McCarty, G.W., Moglen, G.E., and Evenson, G.R. 2018. Assessing the cumulative impacts of geographically isolated wetlands on watershed hydrology using the SWAT model coupled with improved wetland modules. J Environ Manage, **223**: 37-48. doi:10.1016/j.jenvman.2018.06.006.

Legates, D.R., and McCabe, G.J. 1999. Evaluating the use of "goodness-of-fit" Measures in hydrologic and hydroclimatic model validation. Water Resources Research, **35**(1): 233-241. doi:10.1029/1998wr900018.

Li, S., Elliott, J.A., Tiessen, K.H., Yarotski, J., Lobb, D.A., and Flaten, D.N. 2011. The effects of multiple beneficial management practices on hydrology and nutrient losses in a small watershed in the Canadian prairies. J Environ Qual, **40**(5): 1627-1642. doi:10.2134/jeq2011.0054.

Liu, M., Huang, C., Wang, L., Zhang, Y., and Luo, X. 2020. Short-Term Soil Moisture Forecasting via Gaussian Process Regression with Sample Selection. Water, **12**(11): 3085. doi:10.3390/w12113085.

López-Ballesteros, A., Senent-Aparicio, J., Srinivasan, R., and Pérez-Sánchez, J. 2019. Assessing the Impact of Best Management Practices in a Highly Anthropogenic and Ungauged Watershed Using the SWAT Model: A Case Study in the El Beal Watershed (Southeast Spain). Agronomy, **9**(10): 576. Available from https://www.mdpi.com/2073-4395/9/10/576 [accessed.

Maheu, A., Anctil, F., Gaborit, É., Fortin, V., Nadeau, D.F., and Therrien, R. 2018. A field evaluation of soil moisture modelling with the Soil, Vegetation, and Snow (SVS) land surface model using evapotranspiration observations as forcing data. Journal of Hydrology, **558**: 532-545. doi:10.1016/j.jhydrol.2018.01.065.

Mahmood, T.H., and Vivoni, E.R. 2011. Breakdown of hydrologic patterns upon model coarsening at hillslope scales and implications for experimental design. Journal of Hydrology, **411**(3-4): 309-321. doi:10.1016/j.jhydrol.2011.10.011.

Manitoba Agricultural Services Corporation (MASC). 2021. Annual Report.

Manitoba Land Initiative. 2001. Province of Manitoba | Manitoba Conservation | Manitoba Land Initiative. (https://mli2.gov.mb.ca) [accessed May 5, 2021, .

Martínez García, G., Pachepsky, Y.A., and Vereecken, H. 2014. Effect of soil hydraulic properties on the relationship between the spatial mean and variability of soil moisture. Journal of Hydrology, **516**: 154-160. doi:10.1016/j.jhydrol.2014.01.069.

Matile, G.L.D., and Keller, G.R. 2012. Subsurface Phanerozoic geology of southern Manitoba, Transect 15 (5500870N). Manitoba Innovation, Energy and Mines, Manitoba GEological Survey Stratigraphic Map SM2012-1, scale 1:600 000.

Mazrooei, A., Sankarasubramanian, A., and Lakshmi, V. 2020. Technical Note: Evaluation of the skill in monthly-to-seasonal soil moisture forecasting based on SMAP satellite observations over the southeastern US. Hydrology and Earth System Sciences, **24**(3): 1073-1079. doi:10.5194/hess-24-1073-2020.

Meagher, M. 2017. The potential benefits of satellite provided soil moisture data [online]. Strategic analysis paper [cited].

Meng, F., Luo, M., Sa, C., Wang, M., and Bao, Y. 2021. Quantitative assessment of the effects of climate, vegetation, soil and groundwater on soil moisture spatiotemporal variability in the Mongolian Plateau. Sci Total Environ, **809**: 152198. doi:10.1016/j.scitotenv.2021.152198.

Michalyna, W., Podolsky, G., and Jacques, E.S. 1988. Soils of the rural municipalities of Grey, Dufferin, Roland, Thompson and part of Stanley. [Soil report]. Canada Manitoba Soil Survey, Soils Report No. D60.: 202 pp. + maps.

Mila, A.L., and Yang, X.B. 2008. Effects of Fluctuating Soil Temperature and Water Potential on Sclerotia Germination and Apothecial Production of Sclerotinia sclerotiorum. Plant disease, **92**(1): 78-82. doi:10.1094/PDIS-92-1-0078.

Moriasi, D.N., Arnold, J.G., Van Liew, M.W., Bingner, R.L., Harmel, D.R., and Veith, T.L. 2006. Model Evaluation Guidelines for Systematic Quantification of Accuracy in Watershed Simulations. American Society of Agricultural and Biological Engineers ISSN 0001−2351, **50**(3): 885-900.

Motisi, A., Rossi, F., Consoli, S., Papa, R., Minacapilli, M., Rallo, G., Cammalleri, C., and D'Urso, G. EDDY COVARIANCE AND SAP FLOW MEASUREMENT OF ENERGY AND MASS EXCHANGES OF WOODY CROPS IN A MEDITERRANEAN ENVIRONMENT. *In* 2012. International Society for Horticultural Science (ISHS), Leuven, Belgium. pp. 121-127.

Mualem, Y. 1976. A new model for predicting the hydraulic conductivity of unsaturated porous media. Water Resources Research, **12**(3): 513-522. doi:10.1029/WR012i003p00513.

Müller, L., Lipiec, J., Kornecki, T., and Gebhardt, S. 2011. Trafficability and workability of soils. Encyclopedia of agrophysics. Dordrecht: Springer: 912-924.

Myneni, R., Knyazikhin, Y., and Park, T. 2015. MCD15A2H MODIS/Terra+Aqua leaf Area Index/FPAR 8-day L4 Global 500m SIN Grid V006 [Data set]. . NASA EOSDIS Land Processes DAAC. doi:https://doi.org/10.5067/MODIS/MCD15A2H.006.

Niehaus, J.P. 2015. Report, Gridded Snow Water Equivalent Data Set Development – Processing Methods Using the Geospatial Data Abstraction Library [User manual]. **DSO-2014-04**.

Ojo, E.R., Bullock, P.R., L'Heureux, J., Powers, J., McNairn, H., and Pacheco, A. 2015. Calibration and Evaluation of a Frequency Domain Reflectometry Sensor for Real-Time Soil Moisture Monitoring. Vadose Zone Journal, **14**(3): vzj2014.2008.0114. doi:10.2136/vzj2014.08.0114.

Oliveira, L., Cecílio, R., Zanetti, S., Loos, R., Bressiani, D., and Srinivasan, R. 2020. Hydrological simulation of a small forested catchment under different land use and forest management [Research Articles]. iForest - Biogeosciences and Forestry, **13**(4): 301-308. doi:10.3832/ifor3221-013.

Pardo Lara, R., Berg, A.A., Warland, J., and Parkin, G. 2021. Implications of measurement metrics on soil freezing curves: A simulation of freeze–thaw hysteresis. Hydrological Processes, **35**(7). doi:10.1002/hyp.14269.

Raddatz, R.L., and Cummine, J.D. 2003. Inter-annual Variability of Moisture Flux from the Prairie Agro-ecosystem: Impact of Crop Phenology on the Seasonal Pattern of Tornado Days. Boundary-layer meteorology, **106**(2): 283-295. doi:10.1023/A:1021117925505.

Raddatz, R.L., Shaykewich, C.F., and Bullock, P.R. 1994. Prairie crop yield estimates from modelled phenological development and water use. Canadian journal of plant science, **74**(3): 429-436. doi:10.4141/cjps94-080.

Rahman, M., Sulis, M., and Kollet, S.J. 2014. The concept of dual-boundary forcing in land surface-subsurface interactions of the terrestrial hydrologic and energy cycles. Water Resources Research, **50**(11): 8531-8548. doi:10.1002/2014wr015738.

Rallo, G., Agnese, C., Minacapilli, M., and Provenzano, G. 2012. Comparison of SWAP and FAO Agro-Hydrological Models to Schedule Irrigation of Wine Grapes. Journal of irrigation and drainage engineering, **138**(7): 581-591. doi:10.1061/(ASCE)IR.1943-4774.0000435.

Refsgaard, J.C. 1997. Parameterisation, calibration, and validation of distributed hydrological models. Journal of Hydrology, **198**(1): 69-97.

Richardson, C.W., Bucks, D.A., and Sadler, E.J. 2008. The Conservation Effects Assessment Project benchmark watersheds: Synthesis of preliminary findings. Journal of Soil and Water Conservation, **63**(6): 590-604. doi:10.2489/jswc.63.6.590.

Romano, N. 2014. Soil moisture at local scale: Measurements and simulations. Journal of Hydrology, **516**: 6-20. doi:10.1016/j.jhydrol.2014.01.026.

Rong, L., Duan, X., Feng, D., and Zhang, G. 2017. Soil Moisture Variation in a Farmed Dry-Hot Valley Catchment Evaluated by a Redundancy Analysis Approach. Water, **9**(2): 92. doi:10.3390/w9020092.

Rosenbaum, U., Bogena, H.R., Herbst, M., Huisman, J.A., Peterson, T.J., Weuthen, A., Western, A.W., and Vereecken, H. 2012. Seasonal and event dynamics of spatial soil moisture patterns at the small catchment scale. Water Resources Research, **48**(10). doi:10.1029/2011wr011518.

Rößler, O., and Löffler, J. 2010. Potentials and limitations of modelling spatio-temporal patterns of soil moisture in a high mountain catchment using WaSiM-ETH. Hydrological Processes: n/a-n/a. doi:10.1002/hyp.7663.

Santhi, C., Arnold, J.G., Williams, J.R., Dugas, W.A., Srinivasan, R., and Hauck, L.M. 2001. Validation of SWAT model on a large river basin with point and non point sources. Journal of the American Water Resources Association, **37**(5).

Schaap, M.G., Leij, F.J., and van Genuchten, m.T. 2001. ROSETTA: a computer program for estimating soil hydraulic paramters with heirarchical pedotransfer functions. Journal of Hydrology, **251**: 163-176.

Schwärzel, K., Menzer, A., Clausnitzer, F., Spank, U., Häntzschel, J., Grünwald, T., Köstner, B., Bernhofer, C., and Feger, K.-H. 2009. Soil water content measurements deliver reliable estimates of water fluxes: A comparative study in a beech and a spruce stand in the Tharandt forest (Saxony, Germany). Agricultural and Forest Meteorology, **149**(11): 1994-2006. doi:10.1016/j.agrformet.2009.07.006.

Seneviratne, S.I., Corti, T., Davin, E.L., Hirschi, M., Jaeger, E.B., Lehner, I., Orlowsky, B., and Teuling, A.J. 2010. Investigating soil moisture–climate interactions in a changing climate: A review. Earth-Science Reviews, **99**(3-4): 125-161. doi:10.1016/j.earscirev.2010.02.004.

Sentelhas, P.C., Gillespie, T.J., and Santos, E.A. 2010. Evaluation of FAO Penman–Monteith and alternative methods for estimating reference evapotranspiration with missing data in Southern Ontario, Canada. Agricultural Water Management, **97**(5): 635-644. doi:10.1016/j.agwat.2009.12.001.

Sparks, A.H. 2018. nasapower: A NASA POWER Global Meterology, Surface SOlar Energy and CLimatology Data Client for R. The Journal of Open Source Software, **3**(30): 1035. doi:10.21105/joss.

Srivastava, A., Saco, P.M., Rodriguez, J.F., Kumari, N., Chun, K.P., and Yetemen, O. 2020. The role of landscape morphology on soil moisture variability in semi-arid ecosystems. Hydrological Processes, **35**(1). doi:10.1002/hyp.13990.

Srivastava, P.K., Petropoulos, G.P., and Kerr, Y.H. 2016. Satellite Soil Moisture Retrieval : Techniques and Applications. Elsevier, San Diego, UNITED STATES.

Stevens Water Monitoring Systems. 2008. The Hydra Probe (R) soil sensor: Comprehensive Stevens Hydra Probe users manual, Stevens Water Monitoring Systems, Beaverthon, OR. doi:http://www.fondriest.com/pdf/stevens_hydra_manual.pdf (acceessed 16 June 2014).

Sunohara, M.D., Gottschall, N., Wilkes, G., Craiovan, E., Topp, E., Que, Z., Seidou, O., Frey, S.K., and Lapen, D.R. 2015. Long-Term Observations of Nitrogen and Phosphorus Export in Paired-Agricultural Watersheds under Controlled and Conventional Tile Drainage. J Environ Qual, **44**(5): 1589-1604. doi:10.2134/jeq2015.01.0008.

Tavakoli, M., and De Smedt, F. 2012. Validation of soil moisture simulation with a distributed hydrologic model (WetSpa). Environmental Earth Sciences, **69**(3): 739-747. doi:10.1007/s12665-012-1957-8.

Tecplot Inc. 2011. *TECPLOT*. Washington: Bellevue.

Therrien, R., McLaren, R., Sudicky, E., and Panday, S. 2010. A three-dimensional numerical model describing fully-integrated subsurface and surface flow and solute transport. User Guide.

van Genuchten, M.T. 1980. A closed-form equation for predicting the hydraulic conductivity of unsaturated soils. Soil Sci. Soc. Am. J.,, **44**: 892-898.

Van Hateren, T.C., Chini, M., Matgen, P., and Teuling, A.J. 2021. Ambiguous Agricultural Drought: Characterising Soil Moisture and Vegetation Droughts in Europe from Earth Observation. Remote Sensing, **13**(10): 1990. Available from https://www.mdpi.com/2072-4292/13/10/1990 [accessed.

Van Liew, M.W., Arnold, J.G., and Garbrecht, J.D. 2003. HYDROLOGIC SIMULATION ON AGRICULTURAL WATERSHEDS: CHOOSING BETWEEN TWO MODELS. Transactions of the ASAE, **46**(6): 1539-1551. doi:10.13031/2013.15643.

Vereecken, H., Huisman, J.A., Bogena, H., Vanderborght, J., Vrugt, J.A., and Hopmans, J.W. 2008. On the value of soil moisture measurements in vadose zone hydrology: A review. Water Resources Research, **44**(4). doi:10.1029/2008wr006829.

Vrugt, J.A., Bouten .W, and Weerts, A. H.,. 2001. Information Content of Data for Identifying Soil Hydraulic Parameters from Outflow Experiments. Soil Sci. Soc. Am. J.,, **65**: 19-27.

Walker, B.D. 2012. Agri-Environmental Monitoring – Manitoba: Methodology and landscape descriptions. Agriculture and Agri-Food Canada, Agri-Environmental Services Branch. Winnipeg, MB and Ottawa, ON: 29 pp.

Wasko, C., Nathan, R., and Peel, M.C. 2020. Changes in Antecedent Soil Moisture Modulate Flood Seasonality in a Changing Climate. Water Resources Research, **56**(3). doi:10.1029/2019wr026300.

Western, A.W., Grayson, R.B., and Blöschl, G. 2002. Scaling of Soil Moisture: A Hydrologic Perspective. Annual Review of Earth and Planetary Sciences, **30**(1): 149-180. doi:10.1146/annurev.earth.30.091201.140434.

Willmott, C.J. 1981. ON THE VALIDATION OF MODELS. Physical Geography, **2**(2): 184-194. doi:10.1080/02723646.1981.10642213.

Zehe, E., Graeff, T., Morgner, M., Bauer, A., and Bronstert, A. 2010. Plot and field scale soil moisture dynamics and subsurface wetness control on runoff generation in a headwater in the Ore Mountains. Hydrology and Earth System Sciences, **14**(6): 873-889. doi:10.5194/hess-14-873-2010.

Zhang, X., Tang, Q., Liu, X., Leng, G., and Li, Z. 2017. Soil Moisture Drought Monitoring and Forecasting Using Satellite and Climate Model Data over Southwestern China. Journal of Hydrometeorology, **18**(1): 5-23. doi:10.1175/jhm-d-16-0045.1.

Zhang, Y., and Wegehenkel, M. 2006. Integration of MODIS data into a simple model for the spatial distributed simulation of soil water content and evapotranspiration. Remote Sensing of Environment, **104**(4): 393-408. doi:10.1016/j.rse.2006.05.011.

Zhang, Y., and Schaap, M.G. 2017. Weighted recalibration of the Rosetta pedotransfer model with improved estimates of hydraulic parameter distributions and summary statistics (Rosetta3). Journal of Hydrology, **547**: 39-53. doi:https://doi.org/10.1016/j.jhydrol.2017.01.004.

Zhu, Q., Wang, Y., and Luo, Y. 2021. Improvement of multi-layer soil moisture prediction using support vector machines and ensemble Kalman filter coupled with remote sensing soil moisture datasets over an agriculture dominant basin in China. Hydrological Processes, **35**(4). doi:10.1002/hyp.14154.

Appendix

Appendix A

Table A.1: Crops grown from 2010 – 2021 in RISMA 4 and RISMA 5 station

Year	RISMA 4 station (sand)	RISMA 5 station (clay)
2010	Canola	Corn
2011	Oats	Canola
2012	Corn	Wheat
2013	Soybeans	Corn
2014	Oats	Soybeans
2015	Corn	Oats
2016	Winter wheat	Soybeans
2017	Soybeans	Oats
2018	Oats	Soybeans
2019	Corn	Oats
2020	Canola	Soybeans
2021	Corn	Wheat

Table A.2: Percentage sand, silt, clay, and bulk density values for soil types at RISMA fields.

Soil type	Depth (cm)	Sand[1] (%)	Silt[1] (%)	Clay[1] (%)	Bulk density[1] (kg/m^3)
KOT	5	90.34	2.28	7.37	1.26
	20	88.11	2.05	9.84	1.54
	50	88.54	1.85	9.61	1.61
	100	84.43	6.05	9.52	1.62
SCY	5	42.16	21.86	35.98	1.46
	20	18.31	19.29	62.4	1.35

50	7.56	25.64	66.8	1.3
100	1.94	27.66	70.4	1.23

[1]The percent values of sand, silt, clay, and bulk density were obtained from Walker, (2012)

Appendix B

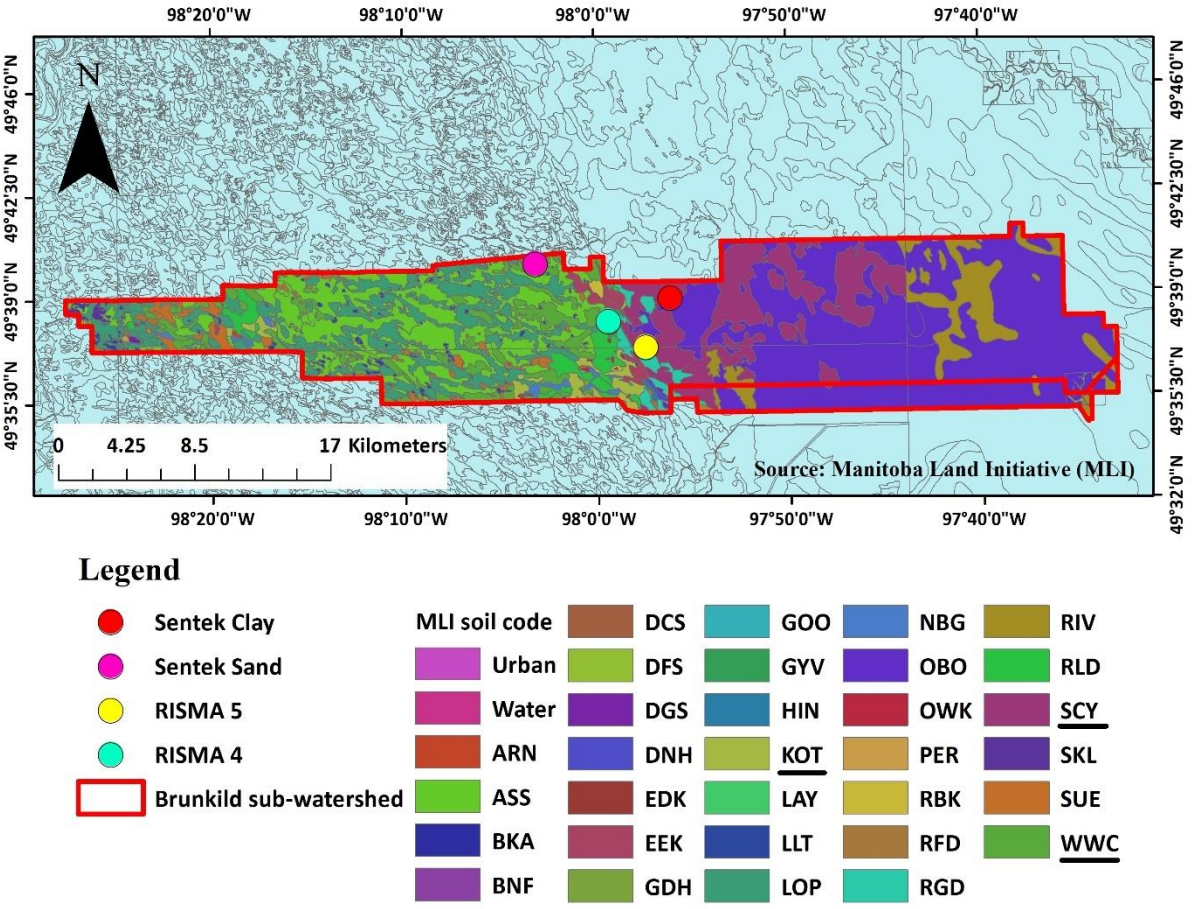

Fig. B.1: Brunkild sub-catchment along with observational fields with MLI as base map

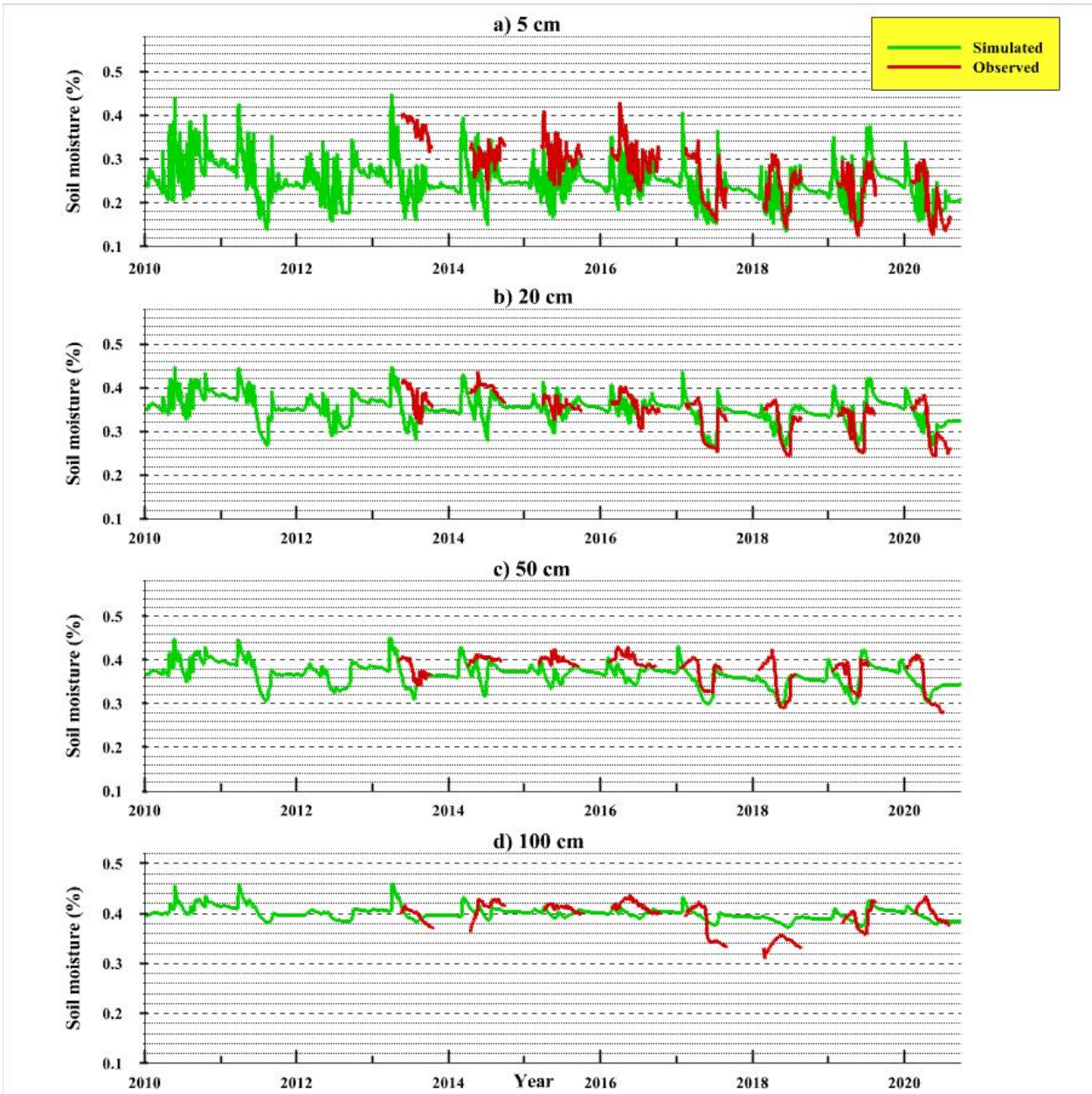

Fig. B.2: Time series graph representing calibration (2010 – 2020) results for simulated vs observed soil moisture at a) 5 cm, b) 20 cm, c) 50 cm, and d) 100 cm depth, for SCY soil series in RIMSA 5 using the 1D model.

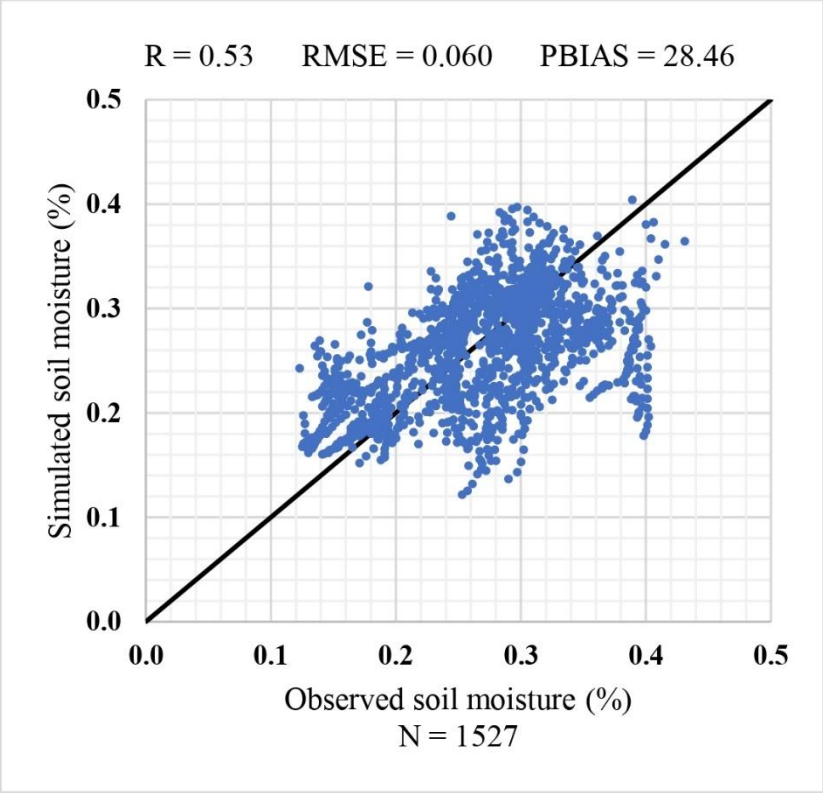

Fig. B.3a: Graphical representation of simulated vs observed surface soil moisture in the SCY soil series using the 3D model

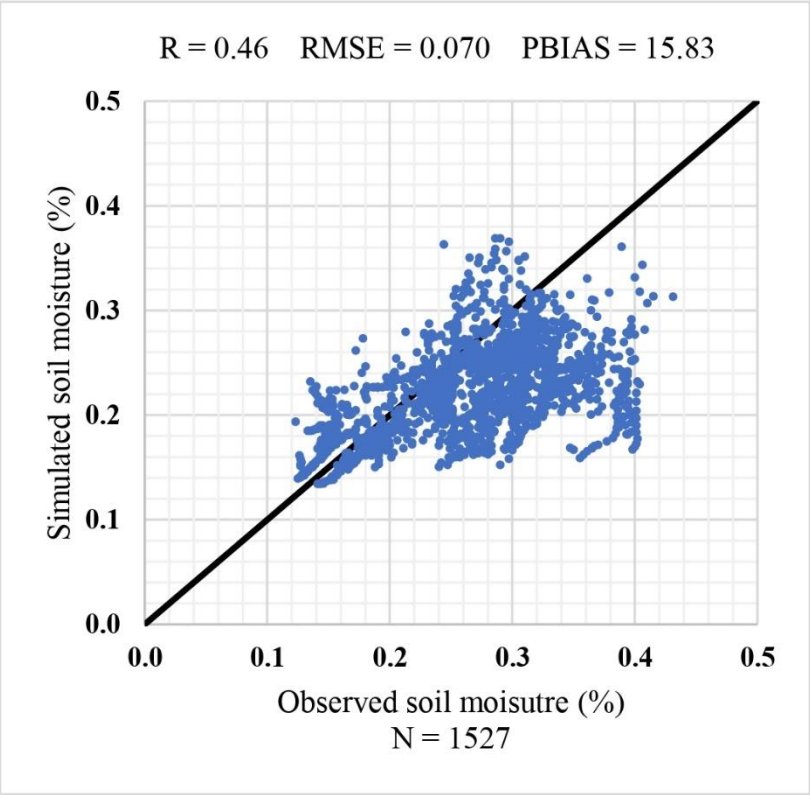

Fig. B.3b: Graphical representation of simulated vs observed surface soil moisture in the SCY soil series using the 1D model.

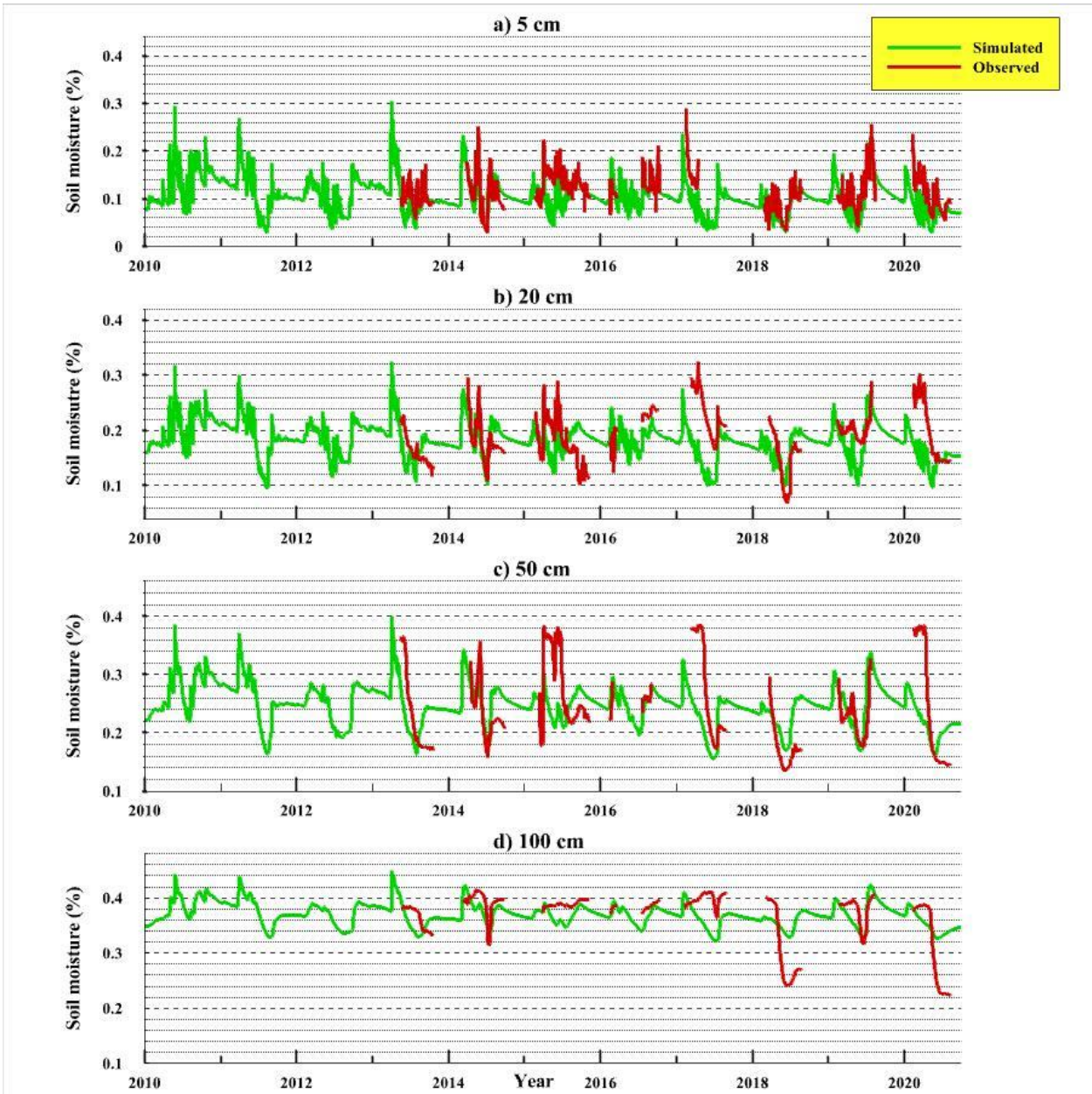

Fig. B.4: Time series graph representing calibration (2010 – 2020) results for simulated vs observed soil moisture at a) 5 cm, b) 20 cm, c) 50 cm, and d) 100 cm depth, for the KOT soil series at RISMA 4 using the 1D model.

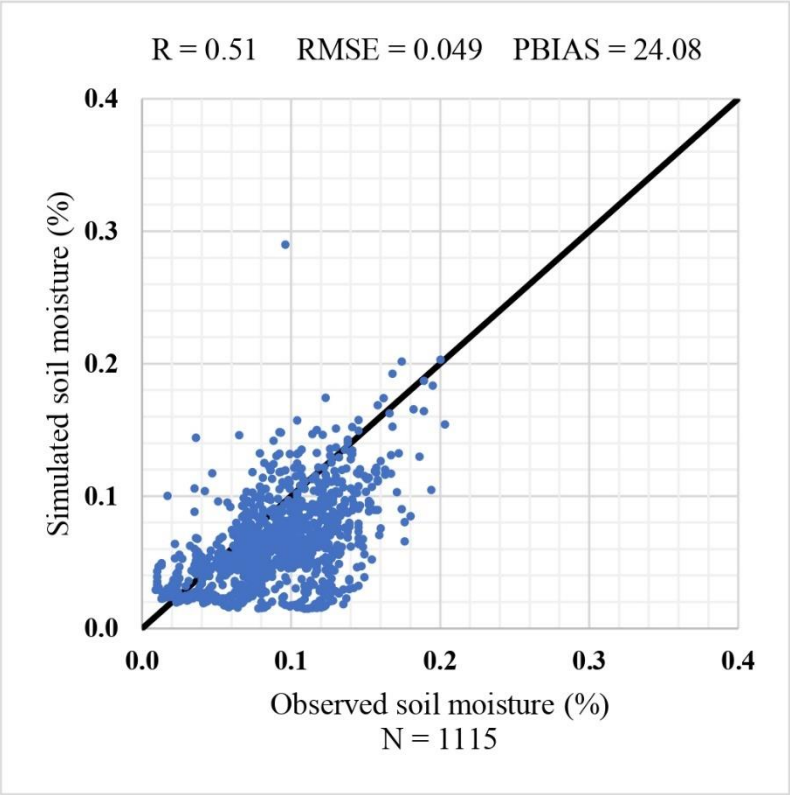

Fig. B.5a: Graphical representation of simulated vs observed surface soil moisture in the KOT soil series using the 3D model.

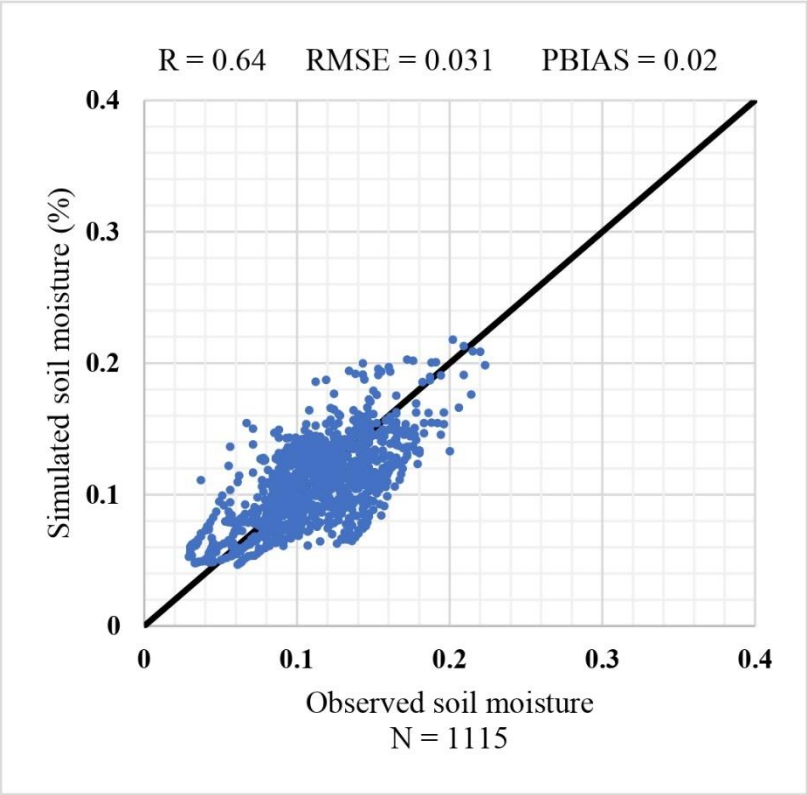

Fig. B.5b: Graphical representation of simulated vs observed surface soil moisture in the KOT soil series using the 1D model.

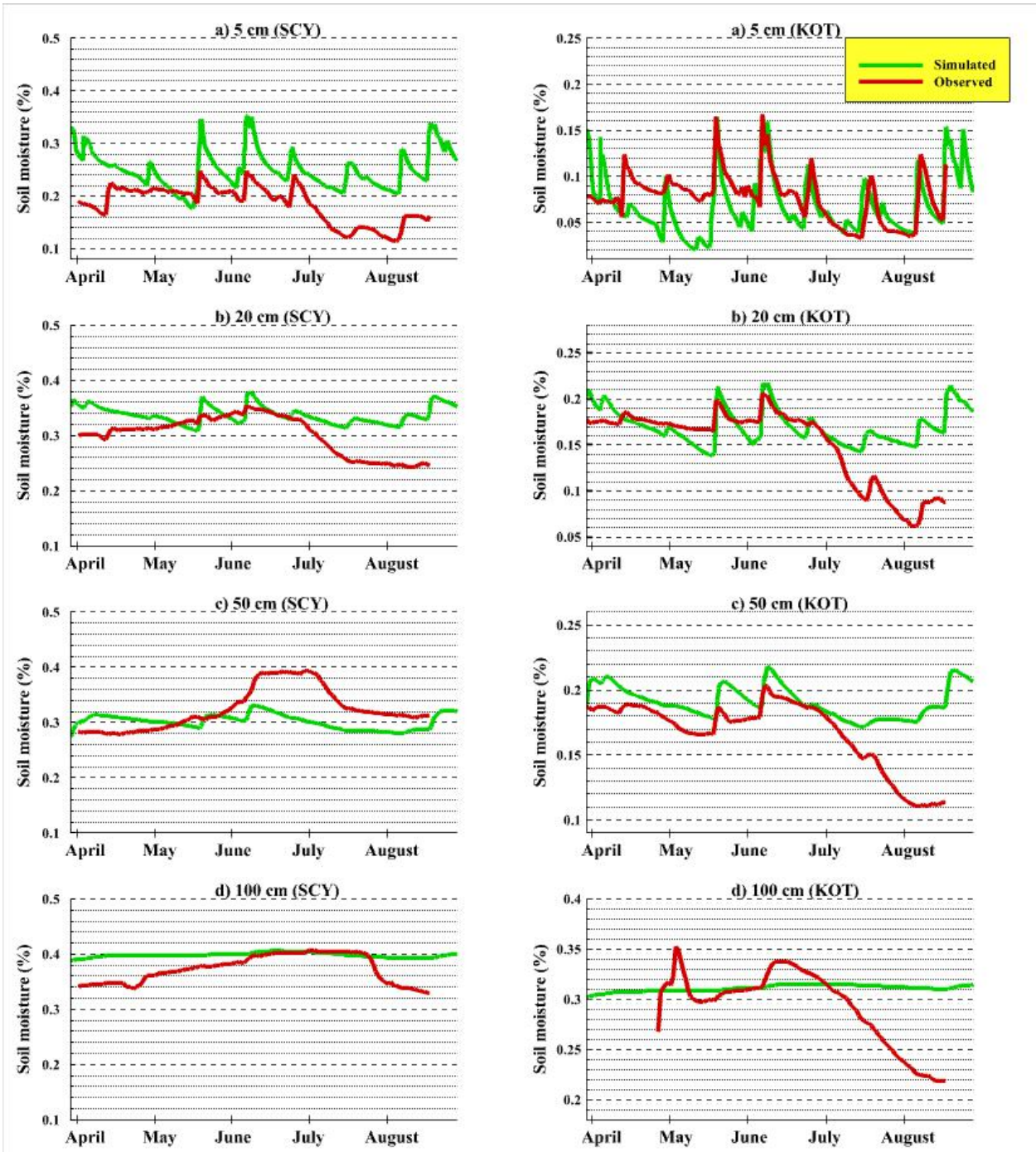

Fig. B.6: Time series graphs presenting forecast results for the 2021 growing season for simulated vs observed soil moisture at a) 5 cm, b) 20 cm, c) 50 cm, d) 100 cm depth, for the SCY and KOT soil series at RISMA 5 and 4, respectively using the 3D model

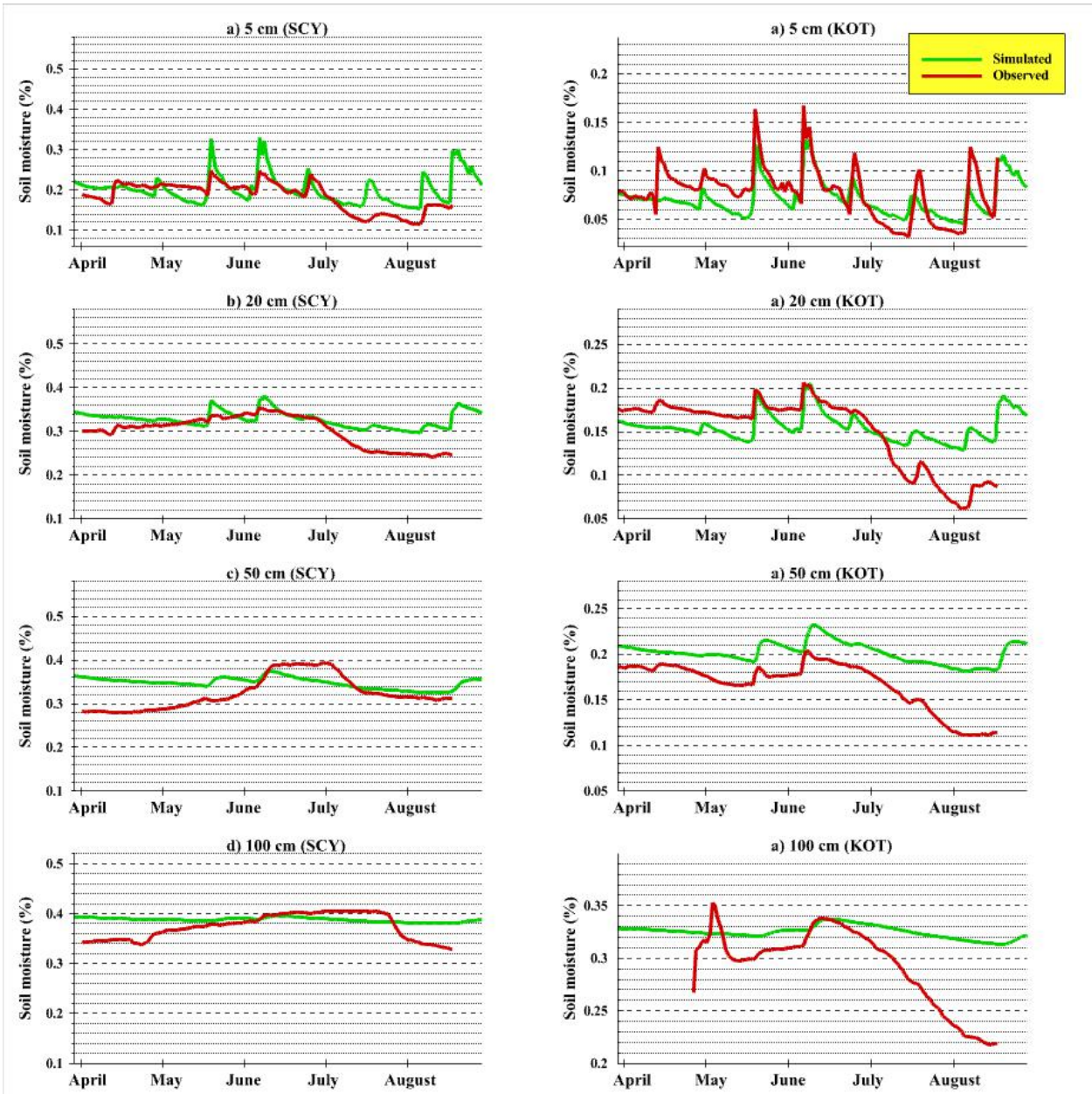

Fig. B.7: Time series graphs presenting forecast results for the 2021 growing season for simulated vs observed soil moisture at a) 5 cm, b) 20 cm, c) 50 cm, d) 100 cm depth, for the SCY and KOT soil series at RISMA 5 and 4, respectively using the 1D model

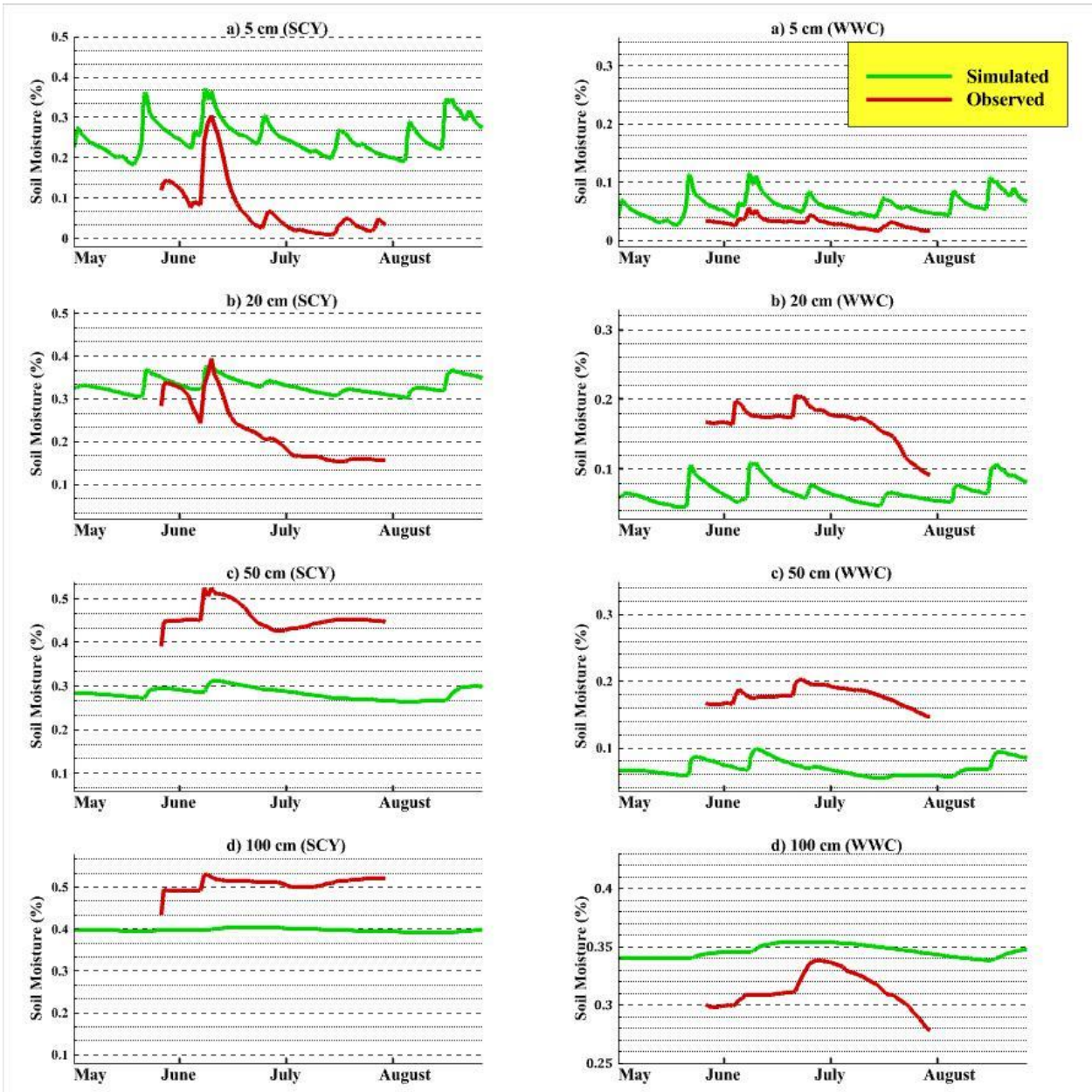

Fig. B.8: Time series graphs presenting forecast results for the 2021 growing season for simulated vs observed soil moisture at a) 5 cm, b) 20 cm, c) 50 cm, d) 100 cm depth, for the SCY and WWC soil series at Sentek Clay and Sentek Sand, respectively using the 3D model